Heliyon 10 (2024) e30528

Contents lists available at ScienceDirect

Heliyon

journal homepage: www.cell.com/heliyon

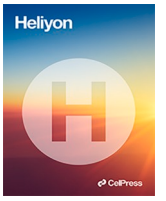

Research article

Customized *m*-RCNN and hybrid deep classifier for liver cancer segmentation and classification

Rashid Khan [a,b,c,1], Liyilei Su [a,b,c,1], Asim Zaman [d], Haseeb Hassan [d], Yan Kang [b,d,**], Bingding Huang [a,c,*]

[a] College of Applied Sciences, Shenzhen University, Shenzhen, 518060, China
[b] Guangdong Key Laboratory for Biomedical Measurements and Ultrasound Imaging, National-Regional Key Technology Engineering Laboratory for Medical Ultrasound, School of Biomedical Engineering, Shenzhen University Medical School, Shenzhen, 518060, China
[c] College of Big Data and Internet, Shenzhen Technology University, Shenzhen, 518188, China
[d] College of Health Science and Environmental Engineering, Shenzhen Technology University, Shenzhen, 518188, China

ARTICLE INFO

Keywords:
Liver cancer classification
Medical image segmentation
cm-RCNN
AHE and e-MBP

ABSTRACT

Diagnosing liver disease presents a significant medical challenge in impoverished countries, with over 30 billion individuals succumbing to it each year. Existing models for detecting liver abnormalities suffer from lower accuracy and higher constraint metrics. As a result, there is a pressing need for improved, efficient, and effective liver disease detection methods. To address the limitations of current models, this method introduces a deep liver segmentation and classification system based on a Customized Mask-Region Convolutional Neural Network (cm-RCNN). The process begins with preprocessing the input liver image, which includes Adaptive Histogram Equalization (AHE). AHE helps dehaze the input image, remove color distortion, and apply linear transformations to obtain the preprocessed image. Next, a precise region of interest is segmented from the preprocessed image using a novel deep strategy called cm-RCNN. To enhance segmentation accuracy, the architecture incorporates the ReLU activation function and the modified sigmoid activation function. Subsequently, a variety of features are extracted from the segmented image, including ResNet features, shape features (area, perimeter, approximation, and convex hull), and enhanced median binary pattern. These extracted features are then used to train a hybrid classification model, which incorporates classifiers like SqueezeNet and DeepMaxout models. The final classification outcome is determined by averaging the scores obtained from both classifiers.

1. Introduction

The liver is the most vital organ in the human abdomen. Liver cancer, a malignant tumour that develops in the liver, is a severe public health issue and one of the most common malignant tumors worldwide [1]. Laparoscopic parenchyma-sparing liver resection, allowing for aggressive excision while preserving as much of the liver as possible, reduces the risk of postoperative liver damage [2].

* Corresponding author. College of Applied Sciences, Shenzhen University, Shenzhen, 518060, China.
** Corresponding author. Guangdong Key Laboratory for Biomedical Measurements and Ultrasound Imaging, National-Regional Key Technology Engineering Laboratory for Medical Ultrasound, School of Biomedical Engineering, Shenzhen University Medical School, Shenzhen 518060, China.
E-mail addresses: kangyan@sztu.edu.cn (Y. Kang), huangbingding@sztu.edu.cn (B. Huang).
[1] These author contributed equally to this work.

https://doi.org/10.1016/j.heliyon.2024.e30528
Received 30 December 2023; Received in revised form 28 April 2024; Accepted 29 April 2024
Available online 6 May 2024

This necessitates careful planning involving resection margin evaluation and the segmentation of liver structures from medical images through the creation of Patient-Specific 3D Models (PSM) [3]. Computed Tomography (CT) is the preferred imaging technique that has gained popularity due to its superior non-ionizing radiation and its ability to provide better lesion-to-liver contrast, among other benefits [4]. Liver segmentation is challenged by factors such as scale diversity, complex backgrounds, unclear borders, and poor contrast in organ density. Accurate liver segmentation can significantly enhance medical evaluation and research [5]. Proper detection and treatment of liver cancer can substantially reduce mortality rates and improve survival prospects [6]. Liver disease, due to its poor prognosis, ranks as the third leading cause of lesion-related mortality, often because it is diagnosed too late [7].

Recently developed, the computerized tumor classification approaches currently employed often do not accurately capture the characteristics observed in the early stages of the disease [8,9]. Deeper neural (DL) networks, though useful for classification, are impractical due to time constraints. Alternatively, shape-based strategies using historical data show promise [10,11]. AI-driven Deep Learning can expedite the creation of PSMs, aiding medical analysis [12]. Despite advancements, clinical validation of AI-generated PSMs remains crucial [13–15]. It is crucial to assess the clinical significance of liver segmentation using automated algorithms, including factors such as the time required to achieve clinically acceptable segmentation [16,17].

Convolutional neural networks (CNNs) excel in image segmentation. A coding-decoding framework, augmented by skip links, minimizes information loss, improving accuracy [18–21].Despite the CNN model's ability to produce highly accurate results, its performance relies on the training characteristics acquired from the dataset. However, precise segmentation and classification of liver cancer are challenging due to the ambiguity of anatomical liver boundaries. Several studies have employed hybrid classification techniques to identify liver cancer in its early stages. However, prior studies have seldom established protocols for estimating liver abnormality levels that may be used for diagnosis and therapy. The majority of the study has concentrated on other data, like disease kind, disease stage, size, number, and progression. Liver function influences the choice of treatment approach in addition to these other parameters. Consequently, to identify liver cancer patients early on and enable quick assessment of liver abnormality levels, we had to have a diagnosis assistance system. This is significant to medical professionals, particularly when it comes to their need for an intelligent system to aid in diagnosis and treatment. In this way, we introduce a novel hybrid deep classifier for liver cancer segmentation and classification using a customized mask-region convolutional neural network (cm-RCNN). The contributions of this work are as follows.

- Proposed a new adaptive histogram equalization (AHE) technique for preprocessing liver images to enhance image contrast.
- The proposed cm-RCNN approach for liver segmentation, which incorporates four max-pooling layers, eight transposed 2D convolutional layers, a dropout layer, ReLU, and the modified sigmoid (*m*-Sig) activation function, efficiently predicts the region mask of the image.
- Inclusion of enhanced median binary pattern (e-MBP)-based features for texture extraction from the segmented image, along with ResNet features and shape features (area, perimeter, approximation, and convex hull).
- Development of a hybrid classification model that combines two classifiers, SqueezeNet and DeepMaxout models, to achieve accurate liver classification.

2. Literature review

In medical image segmentation, several notable contributions have been made towards the accurate delineation of the liver from CT scans, focusing on leveraging deep learning methodologies. MCFA-UNet-based neural network addresses the edge feature loss from minimal feature extraction [22]. Initially, multiscale characteristic data was extracted through multiple simultaneous convolution paths, and dual attention mechanisms were employed to analyze the combined multiscale data from these distinct paths. Subsequently, the attention gate technique was used to merge feature details from specific levels, minimizing semantic differences between the decoding and encoding paths. Finally, a DL approach was applied to improve network segmentation using the characteristic data in the decoding path. In Ref. [12], Automated methods, like preprocessing level sets, optimize segmentation, addressing tumor region identification [5,7].

Furthermore, the method accurately classified liver cancer, facilitating earlier diagnosis. The CNN model utilized a 3×3 kernel size and ReLU activation function, with an extracted feature map processed through a fully connected layer containing 2048 neurons [23]. The SoftMax layer was then employed for binary categorization, demonstrating the model's effectiveness in liver cancer classification.

In addition, Zhang et al. present a liver cancer classification approach using paired labels, which incorporates Transfer Learning (TL)-based Support Vector Machines (SVM) and NH-SVM [8]. NH-SVM is introduced to enhance TL effectiveness related to the target domain. This work demonstrates efficient liver cancer classification compared to other state-of-the-art methods. Balasubramanian et al. developed APESTNet, an approach for liver cancer segmentation and classification utilizing the mask-RCNN technique [10]. Histogram equalization (HE) was initially applied for image preprocessing to enhance contrast. For segmentation, the mask-RCNN approach was employed to isolate the liver region within the image. Additionally, APESTNet was used to address the issue of overfitting. In the context of liver image analysis, a hybrid ResUNet approach for liver segmentation [12]. This hybrid model combined elements of both ResNet and UNet models to effectively extract the region of interest (ROI) from the image. Reddy et al. [24] developed a model to evaluate the performance of convolutional neural networks (CNNs) and support vector machines (SVM) classifiers in the novel liver segmentation classification using CT images. To identify the liver CT picture collection, two classifiers are used: CNN and Support Vector Machine (SVM). For this investigation, twenty samples were gathered and divided into two groups. Group 1 utilized CNN for ten samples, and Group 2 used SVM with 0.8 G power for ten samples. The precise elliptical liver structure is extracted using a 3D Sparse Deep Belief Network with Enriched Seagull Optimization (3D-SDBN-ESO) that was developed by Dickson et al. [25]. The

preparation stage of the liver segmentation procedure begins with the feeding of the abdominal CT images. Here, Gaussian filtering and contrast local adaptive histogram equalization are used. Following preprocessing, high-level spatiotemporal characteristics are extracted to partition the liver in the proposed 3D-SDBN. In addition to providing feature representation, this model efficiently gains high-level contextual information and improves network capacity and performance.

2.1. Problem statement

Table 1 presents the features and challenges of existing liver segmentation and classification techniques. In the case of MCFA-UNet [6], the author successfully minimized the semantic gap in the skip connection. However, implementing advanced ML strategies and lightweight model approaches remains a challenge. For CNN [26], the author achieved better dice scores and precision. Nevertheless, improving the recognition of tiny tumors and enhancing the overall system performance remains a complex task. The use of UNet [7] has reduced the time required for the early diagnosis of liver cancer patients. However, dealing with vascular structures and achieving complete segmentation with lesions poses significant challenges. DL [5] effectively recognizes correct histopathological images with high reliability. Nonetheless, there is a need for clarity in implementing EM-based patch selection and the K-means clustering technique to enhance performance efficiency. In the case of 3D-CNN [23], it effectively captures both the overall and inner framework of various tumor types. However, the incorporation of extracted features within the suggested 3D CNN framework to achieve effective classification presents complexities. SVM [8] enhances hand-crafted characteristics with improved feasibility. Yet, the application of a weighted loss function and data augmentation approaches is essential to address the data imbalance issue. Mask-RCNN [10] successfully avoids overfitting. Nevertheless, there is a need to explore the use of z-axis data in 3D to minimize potential errors. Lastly, with ResUNet [12], a maximal dice coefficient rate has been achieved. However, to further enhance cancer localization precision, it is imperative to delve into DL strategies. SVM [24] minimizes the time for early detection of the liver. However, these systems were deficient in the segmentation and detection of liver lesions due to low contrast between the liver and the neighboring organs. 3D-SDBN [25] accurately segments the liver from abdominal CT images. However, vascular structures must be addressed, and complete segmentation with lesions must be achieved. Moreover, other existing methods for treating liver tumors face many difficult problems, including the fact that other organs surround the liver regions; as a result, the CT values of the liver and surrounding organs are comparable, making tumour analysis more difficult. Identification of the liver tumor boundaries becomes difficult since there is little difference between the liver tumor and healthy tissue, and the margins are hazy. Similar to the shape, location, and size of liver tumors, these difficulties must be addressed to improve the segmentation of the liver and liver tumors. There are numerous differences in the size, location, and kind of liver lesion observed in CT images. The development of a fully automated segmentation system is still a difficult task despite the use of various techniques. This is because of the unpredictable intensity variation between the liver and lesion tissue, as well as variations in contrast and scanner resolution. To overcome these limitations, this work intends to propose a novel hybrid model for segmenting and classifying liver cancer.

3. Proposed methodology

3.1. Liver cancer segmentation and classification

In this study, we introduce a novel framework for liver cancer segmentation and classification, comprising the following key steps: preprocessing, segmentation, feature extraction, and classification. The diagrammatic representation of our proposed framework is illustrated in Fig. 1. The initial stage involves preprocessing the input liver image, employing AHE. Through AHE, the input image rectifies color distortion and applies linear transformations to obtain a well-preprocessed image. The AHE technique follows these

Table 1
Features and challenges of extant techniques for liver segmentation and classification.

Author [citation]	Methodology	Features	Challenges	Date of Publication
Zhou et al. [22]	MCFA-UNet	Minimizes the semantic gap in the skip connection.	Does not incorporate advanced ML strategies and lightweight model approaches.	2023August
Manjunath et al. [26]	CNN	Achieved better dice scores and precision.	Need to enhance recognition of tiny tumors and system performance.	2022 Mar 1
Zhang et al. [8]	SVM, Multi-source TL	Enhances hand-crafted characteristics with more feasibility.	The application of weighted loss function and data augmentation to mitigate data imbalance is required.	2021 Apr 16
Balasubramanian et al. [10]	Mask-RCNN	Avoids overfitting issues.	Integration of z-axis data in 3D to minimize errors needed.	2023 Jan 4
Rahman et al. [12]	ResUNet	Achieved maximal dice coefficient rate.	DL strategy required for improved cancer localization precision.	2022 Aug 5
Reddy et al. [24]	SVM	Minimizes the time for early detection of the liver.	These systems were deficient in segmenting and detecting liver lesions due to low contrast between the liver and the neighboring organs.	2023 Jun 22
Dickson et al. [25]	3D-SDBN	Accurately segments the liver from abdominal CT images.	Vascular structures must be addressed, and complete segmentation with lesions must be achieved.	2023 Jun 1

stages: Dehazing, removal of colour distortion, and linear transformation. The process, known as dehazing, employs the dark channel prior approach to assess and mitigate haze. In the next stage, we eliminate color distortion from the dehazed image, known as color correction or white balancing. Moreover, the colour distortion-corrected image undergoes linear transformation, where pixel values are adjusted or scaled to a new range. Subsequently, we perform liver region segmentation on the preprocessed image, precisely delineating the ROI within the liver. To accomplish this, we utilize an innovative deep strategy called cm-RCNN, enhanced with the ReLU and *m*-Sig activation functions. Our framework then proceeds to extract essential features from the segmented image, including ResNet features, shape features (area, perimeter, approximation, and convex hull), and the e-MBP. The final phase involves training the extracted features using a hybrid classification model, incorporating classifiers such as SqueezeNet and DeepMaxout models. The classification outcome is determined by averaging the scores obtained from both classifiers.

3.2. Preprocessing

Consider an input liver image represented as L^{Img}. This is initially subjected to the preprocessing step to enhance its quality. Preprocessing involves preparing the input image for subsequent validation steps by addressing various aspects such as noise reduction, resizing, contrast enhancement, rotation, cropping, histogram equalization, and more. Numerous techniques are available for image preprocessing, and our approach adopts a novel technique known as AHE.

3.2.1. Proposed AHE for preprocessing

AHE is an extension of the standard histogram equalization (HE) technique, typically employed for contrast improvement in the input image L^{Img}. While standard HE applies a global transformation to the entire image, AHE operates locally on distinct portions of the image, thereby enhancing contrast throughout various regions in the input image L^{Img}. In our proposed AHE technique [27], we follow these stages: Dehazing, removal of color distortion, and linear transformation. The AHE preprocessing technique for the input image is illustrated in Fig. 2.

Input image: Initially, the input image L^{Img} is read and then passed to the dehazing stage.

Dehazing stage: In this stage, the fog or haze is eliminated from the input image L^{Img}. This process, known as dehazing, employs the dark channel prior approach to assess and mitigate haze. The dark channel prior approach involves the following steps:

Step 1. Compute the dark channel of the input image L^{Img}.

Step 2. Estimate the transmission map.

Step 3. Trim the transmission map to ensure accurate values.

Step 4. Retrieve the dehazed image.

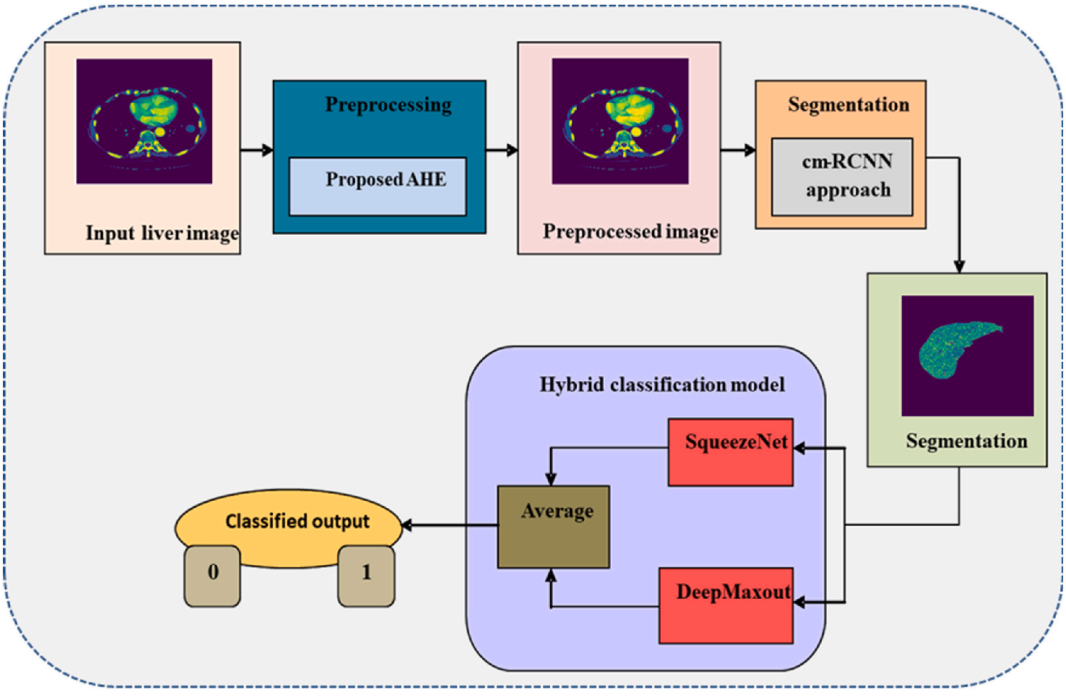

Fig. 1. Diagrammatic representation of the proposed framework.

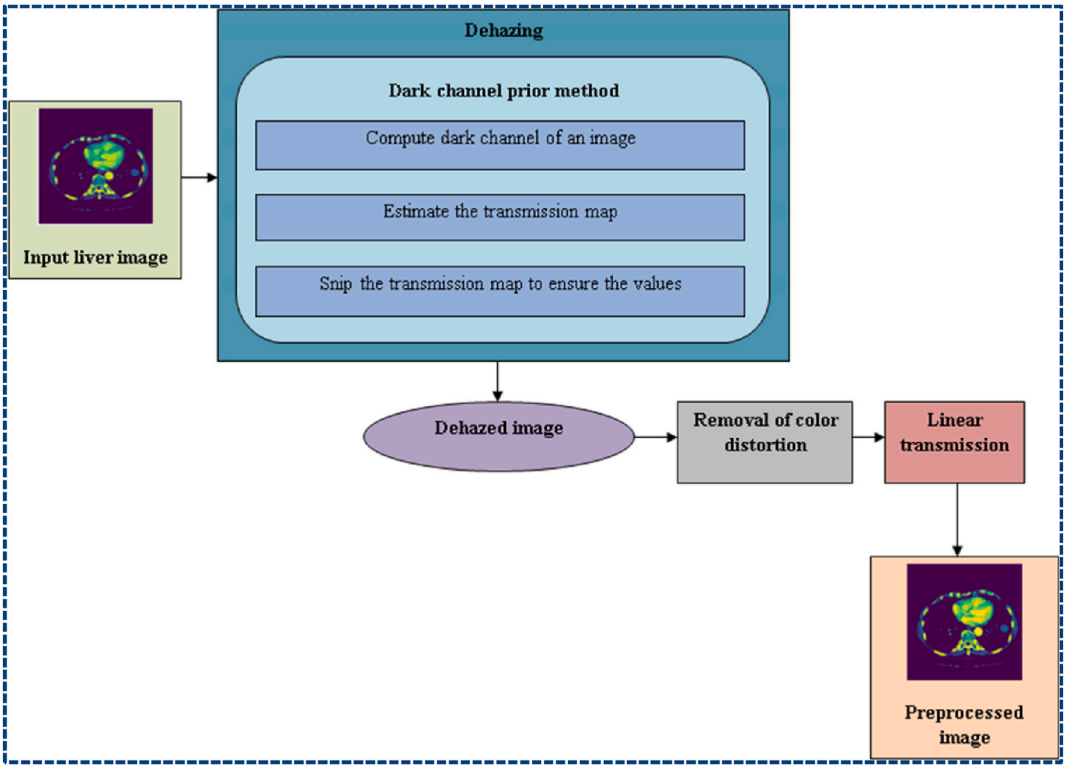

Fig. 2. Proposed Flow of AHE technique for preprocessing the input image.

Removal of color distortion: In this stage, we eliminate color distortion from the dehazed image, a process known as color correction or white balancing. This approach ensures that the mean color in the image is achromatic or grey. It scales the color channels so that the mean of the image aligns with this achromatic value, effectively removing color distortion from the dehazed image.

Linear transformation: The color distortion-corrected image undergoes linear transformation, where pixel values are adjusted or scaled to a new range. This adjustment or scaling of pixel values enhances the contrast of the color-corrected image. We employ a specific linear transformation function, as represented in Eq. (1), to minimize or maximize the grayscale of the image. Here, S_v refers to shift value ($S_v = 1.2$), Sf refers to scaling factor ($Sf = 30$), x refers to original grey values, and LT refers to the resulting values after transformation.

$$LT = S_v * x + Sf \tag{1}$$

This preprocessing using the proposed AHE technique results in the input image being transformed into the preprocessed image I^{pre}.

3.3. Segmentation: proposed cm-RNN architecture

Segmentation is the process of dividing the image into multiple segments, primarily aiming to locate boundaries and objects such as curves and lines. It involves assessing the image I^{pre}'s pixel features to partition it into various regions or segments. In our approach, we propose the use of the cm-RCNN technique for image segmentation. The cm-RCNN approach [28] is a variant of the mask region-based convolutional neural network (*m*-RCNN). The standard framework of *m*-RCNN [29] is depicted in Fig. 3. The preprocessed image I^{pre} is first passed through the backbone network and then input to the region proposal network (RPN), which efficiently selects the ROI. Following this, features are extracted from the RPN and subsequently processed through three 2D convolution layers. These convolutional operations help generate the segmented image as the final output.

The standard *m*-RCNN offers several advantages, including higher efficiency, simplicity, and flexibility for handling various tasks. However, it faces challenges related to overfitting and the detection of fine-grained objects. To address these challenges, we introduce the cm-RCNN model, which is adapted for object detection and rapid segmentation. Fig. 4 illustrates the framework of the proposed cm-RCNN approach. Initially, the backbone network extracts the features from the preprocessed image I^{pre}. This CNN model serves as the backbone network responsible for convolving the features extracted from the image I^{pre}. It includes two 2D convolution layers with dimensions ($256 \times 256 \times 64$) to handle the (256×256) image size with a filter size of 64. It also incorporates a dropout layer with a probability rate of 0.5 and a 2D max-pooling layer with dimension ($128 \times 128 \times 64$). Applying the ROI pooling layer to these bounding boxes makes the entire object equivalent. This process is repeated a total of four times in the backbone network. Then, the extracted

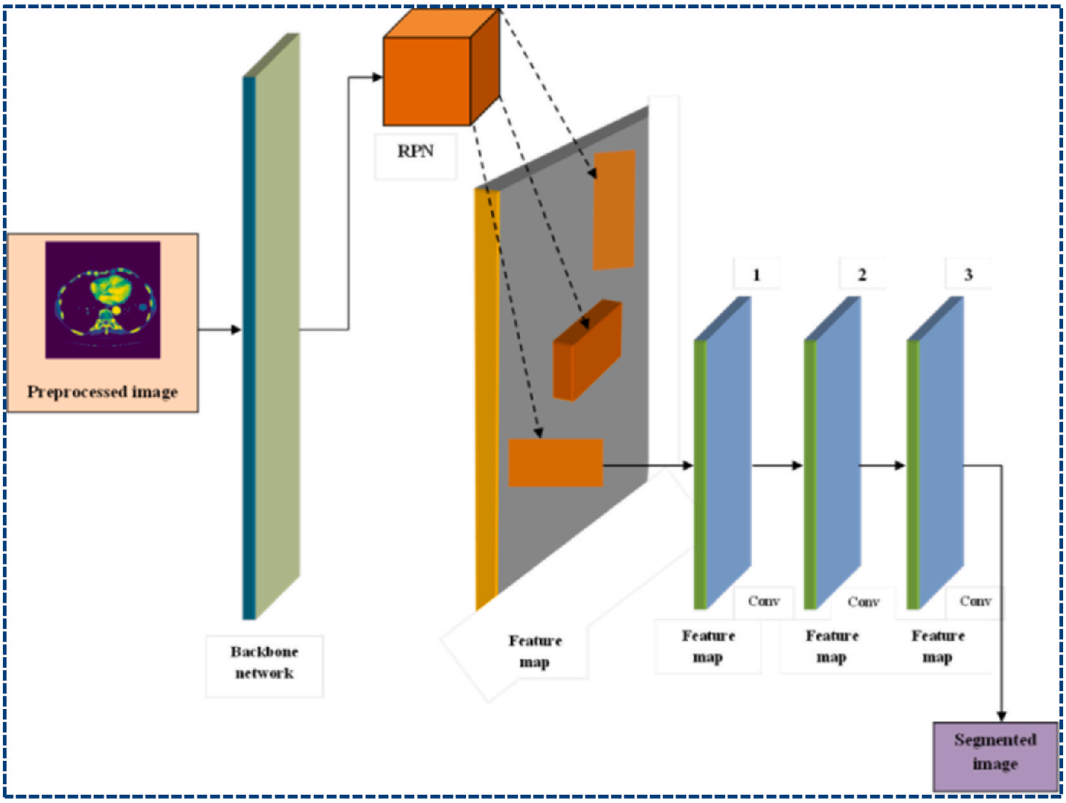

Fig. 3. Standard framework of *m*-RCNN.

features from the backbone network are fed to the RPN, which both produces potential object regions in the image I^{pre} and retrieves features from the backbone network. The RPN comprises five 2D convolutional layers with dimensions $(16 \times 16 \times 512)$ and a filter size of 512. The last three layers of the 2D convolutional layer from the standard *m*-RCNN are incorporated into the mask head layer of the proposed cm-RCNN approach. The proposed approach includes four layers of mask heads, with each mask head featuring three layers of 2D convolutional layers from the standard *m*-RCNN. The specifications for the layers within the four mask heads are as follows:

Mask head 1: The first 2D convolutional layer has dimension $(16 \times 16 \times 512)$, followed by the second transpose 2D convolutional layer with dimensions $(32 \times 32 \times 512)$, a dropout layer with a probability rate of 0.2, and the third transpose 2D convolutional layer with dimensions $(16 \times 16 \times 512)$.

Mask head 2: The first 2D convolutional layer has dimensions $(64 \times 64 \times 256)$, followed by the second transpose 2D convolutional layer with dimensions $(128 \times 128 \times 256)$, a dropout layer with a probability rate of 0.2, and the third transpose 2D convolutional layer with dimensions $(256 \times 256 \times 256)$.

Mask head 3: The first 2D convolutional layer has dimensions $(256 \times 256 \times 128)$, followed by the second transpose 2D convolutional layer with dimensions $(512 \times 512 \times 128)$, a dropout layer with a probability rate of 0.2, and the third transpose 2D convolutional layer with dimensions $(1024 \times 1024 \times 6)$.

Mask head 4: The first 2D convolutional layer has dimension $(16 \times 16 \times 12)$, followed by the second transpose 2D convolutional layer with dimensions $(16 \times 16 \times 4)$, a dropout layer with a probability rate of 0.2, and the third transpose 2D convolutional layer with dimensions $(4096 \times 4096 \times 1)$.

In total, the proposed cm-RCNN approach utilizes nine feature maps. Notably, while the standard *m*-RCNN incorporates only one pooling layer in the backbone network, our proposed method includes four max-pooling layers and eight transposed 2D convolutional layers in the decoder part. Additionally, a dropout layer is introduced between all 2D convolutional layers during feature extraction and expansion. Furthermore, the ReLU activation function is applied in the proposed work, except for the last layer.

Finally, the extracted features are fed into the fully connected layer to predict the region mask. In the output layer, we employ the *m*-Sig activation function [30], which is a variant of the standard sigmoid activation function. The mathematical formulation of the conventional sigmoid activation is expressed according to Eq. (2).

$$Sig(X) = \frac{1}{1 + e^{-X}} \tag{2}$$

The standard sigmoid activation function is suitable when the network infrastructure is simple, and gradient issues are less pronounced. However, the sigmoid function tends to saturate when the input is negative or positive. To mitigate this issue, we propose the

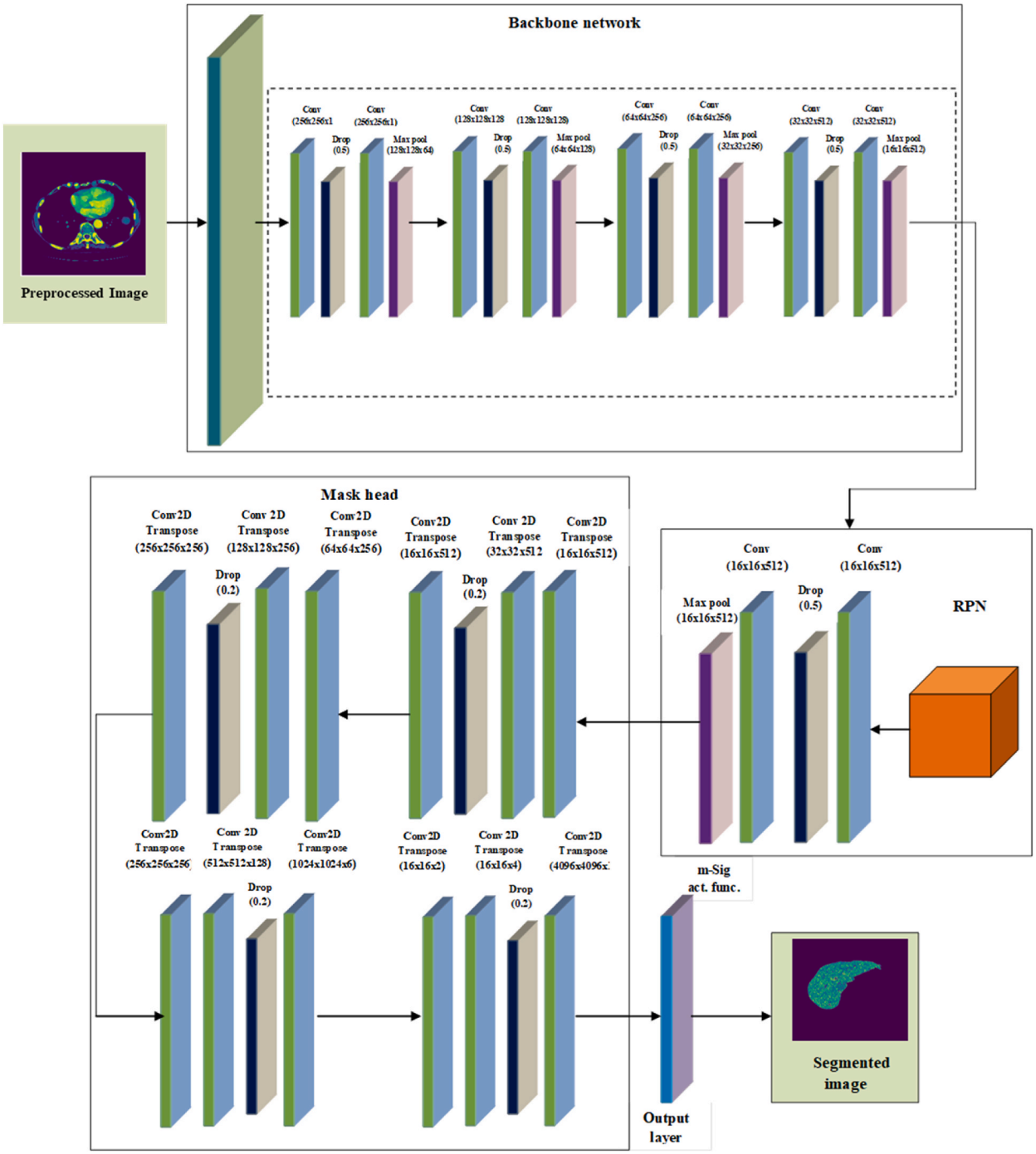

Fig. 4. Framework of proposed cm-RCNN-based segmentation.

m-Sig activation function, the mathematical formulation of which is expressed in Eq. (3). A smooth, continuous function with a clearly defined derivative at each point is the sigmoid function. For gradient-based optimization algorithms used in neural network training, this characteristic is advantageous. When the input varies, smoothness enables more steady and predictable variations in the output. Smoothness, constrained output range, non-linearity, monotonicity, differentiability, historical prevalence, and output stability are just a few of the benefits that the sigmoid function has to offer overall. It is a well-liked option for many applications in logistic regression, neural networks, and other statistical modeling jobs because of these characteristics.

$$m - Sig(X) = \frac{e^{X}}{1 + e^{-X}} + f_X \tag{3}$$

The *m*-Sig activation function is primarily employed to achieve improved classification results, as it maps the input values into the range (0, 1). Consequently, the segmented image can be represented as I^{Seg}.

3.4. Feature extraction: an overview of ResNet feature, shape feature, and e-MBP

Feature extraction transforms the visual format into a numerical form for successful classification. Various feature extraction approaches are available depending on the specific task. For liver cancer classification, we extract ResNet features, shape features (including area, perimeter, approximation, and convex hull), and e-MBP-based features. A detailed explanation of these features is given in Sections 3.4.1–3.4.3.

3.4.1. ResNet feature

The ResNet feature is a critical component of the CNN framework, employing residual connections to enhance information flow through deeper layers. In our approach, ResNet features are extracted from the segmented image I^{Seg}, comprising mean feature vectors obtained from intermediate layers of the pre-trained ResNet model. Therefore, the ResNet features extracted from I^{Seg} can be represented as R_f.

3.4.2. Shape feature

Shape features, as described in Ref. [31], serve to quantitatively represent the geometric characteristics of the region of interest (ROI) or objects within an image. These shape features, including area, perimeter, approximation, and convex hull, are extracted from the segmented image I^{Seg}. An explanation of the shape features is provided below.

Area: Area quantifies the size of a region or object within an image by measuring the pixel count enclosed by its boundary. Larger areas correspond to larger objects, making it useful for distinguishing objects of different sizes.

Perimeter: Perimeter measures the length of the contour or boundary of an object within an image. It aids in assessing the complexity or irregularity of the object's shape. Objects with intricate shapes tend to have longer perimeters.

Approximation: Approximation involves estimating an object's boundary length using a simple geometric shape, typically a polygon such as a minimal enclosing triangle or a minimal bounding triangle. This simplifies complex shapes, making them easier to compare and analyze.

Convex hull: The convex hull represents the smallest convex polygon that fully encloses the object, connecting its outermost points along the contour. It is employed to recognize the object's boundary and overall shape.

The shape-based features extracted from the segmented image can be represented as Shp_f.

3.4.3. e-MBP

e-MBP, a variant of the Median Binary Pattern (MBP) [29] akin to the Local Binary Pattern (LBP), serves as a method for extracting texture features from the segmented image. Distinct from the LBP, which utilizes the central pixel to provide effective sensitivity and increased noise reliability, MBP employs the median value within the image patch, acting as a local threshold. The e-MBP is adopted to extract the texture features from the segmented image I^{Seg}. Mathematically, the traditional MBP is expressed as shown in Eq. (4), where $\tau(i,j)$ refers to the median in the image patch, with values estimated as $\tau(i,j) = median(M_p(i,j))$, and M_p refers to bits in the binary pattern.

$$Mbp_{p,q}(i,j) = \sum\nolimits_{z \in M_p(i,j)} 2^z . H(x_z - \tau(i,j)) \tag{4}$$

The traditional MBP effectively captures texture-relevant details from the segmented image I^{Seg} and provides an accurate feature vector. Nevertheless, it exhibits increased sensitivity to noise, resulting in potentially inaccurate texture extraction. To address this challenge, a novel e-MBP is employed. The mathematical formulation of e-MBP is defined in Eq. (5).

$$e - Mbp = \sum\nolimits_{z \in M_{p_{ij}}} 2^z . H(a_z) \tag{5}$$

Where, M refers to the number of neighbors, and a_z refers to intensity value. Conventionally, the intensity value function is estimated as $f(a_z) = \begin{cases} 1, if\ \ a_z \geq Median \\ 0, otherwise \end{cases}$, which can be replaced with the following intensity value function $f(a_z) = \begin{cases} 1, if\ \ a_z \geq J_{Med} \\ J_{r(i,j)}, if\ \ J_{\min} - \alpha V_B < J_{(i,j)} < J_{Max} - \alpha V_B \\ 0, if [J_{\min} + \alpha V_B < J_{Med} < J_{Max} - \alpha V_B] \\ 0, otherwise \end{cases}$ for accurate classification. Here, $J_{\min}$ refers to the minimum value among neighbors, J_{Med} refers to the median value among neighbors, J_{Max} refers to the maximum value among neighbors, α relates to the control parameter [0, 1] that resolves the median rate, V_B refers to a value that adapts based on the local context, $V_B = sum[pixel\ at\ (i,j)\ intensity -$

Center pixel value], and $J_{r(i,j)} = \begin{cases} 1, if \ \dfrac{\max(GI)}{2} > GI_{(i,j)} \\ 0, otherwise \end{cases}$.

The combined features extracted from the ResNet, shape, and e-MBP-based features can be represented as $E^{Ftrs} = [R_f, Shp_f, e-Mbp]$.

3.5. Proposed hybrid classification model

After extracting the features E^{Ftrs}, the next step is to train these features for efficient liver cancer classification. We propose a hybrid classification model that accelerates the entire classification process by using two or more classifiers. In this work, the hybrid classification model consists of two models: SqueezeNet and DeepMaxout. As illustrated in Fig. 5, the extracted feature set E^{Ftrs} is separately input into both models. The SqueezeNet and DeepMaxout models train the feature set for accurate liver cancer classification, and they produce intermediate scores. Subsequently, the average of scores from both models determines the final classification result, which is either "0" indicating non-cancer or "1" indicating cancer. The probability values of the intermediate scores are above 0.5.

3.5.1. SqueezeNet model

Squeeze Net [27] is a DNN framework designed for efficient model inference, especially suitable for resource-constrained systems. The architecture of SqueezeNet is illustrated in Fig. 6. To train the extracted feature set E^{Ftrs}, we utilize the SqueezeNet model. Initially, the feature E^{Ftrs} is passed through a convolutional layer with a filter size of 96. This convolutional layer employs small kernels or filters to operate on the feature E^{Ftrs}. It performs operations like element-wise multiplication between the overlapping input regions and filters, resulting in convolved values. Following the convolution step, the values undergo pooling with strides of (2×2), which reduces computational complexity by downsampling the feature map. Subsequently, fire module 1 is employed, which is a building block comprising a squeeze layer and an expand layer. The squeeze layer reduces the input channels, while the expand layer increases them.

This design reduces network redundancy and effectively enhances classification. Fire module 1 consists of three layers: layer 0, layer 1, and layer 2, all using the ReLU activation function. It is then passed through a pooling layer with a pool size of three and strides of (2×2). Next, it proceeds to fire module 2, which comprises four layers: layer 3, layer 4, layer 5, and layer 6, all utilizing the ReLU activation function. Following this, it undergoes pooling with a pool size of three and strides of (2×2). Finally, it is directed to fire module 3, which consists of a single layer (layer 7) employing the ReLU activation function. Moreover, it passes through a dropout layer with a rate of 0.5, effectively addressing the overfitting problems. Subsequently, it proceeds to a convolutional layer with a filter size of 1000, followed by a global average layer and a pooling layer. These outputs are then fused in the fully connected layer to generate the intermediate scores. The intermediate score obtained from the SqueezeNet model can be represented as S^{Out}.

3.5.2. DeepMaxout model

The DeepMaxout model [4] is employed in this work to train the input feature set. This model utilizes two critical layers: the dropout and maxout layers, which enhance the precision of liver classification. The DeepMaxout model is composed of various layers, including the input layer, convolution layer, dropout layer, max-pooling layer, maxout unit, embedding layer, and output layer. The convolution layer convolves the feature set E^{Ftrs} to extract features using filters or kernels. The dropout layer selectively deactivates certain neurons for subsequent layers, effectively mitigating the overfitting problem. Subsequently, the max-pooling layer selects the maximum value from a specified area within the feature map, defined by the kernel. The mathematical expression of the maxout unit is represented as shown in Eq. (6).

$$Q\left(E^{Ftrs}\right) = \max_{u \in [1,\delta]} G_{yu} \tag{6}$$

Where u refers to the feature map $G_{yu} = E^{Ftrs}.W_{yu} + \chi_{yu}$, W refers to weight, and χ refers to the bias term. Therefore, the scores obtained

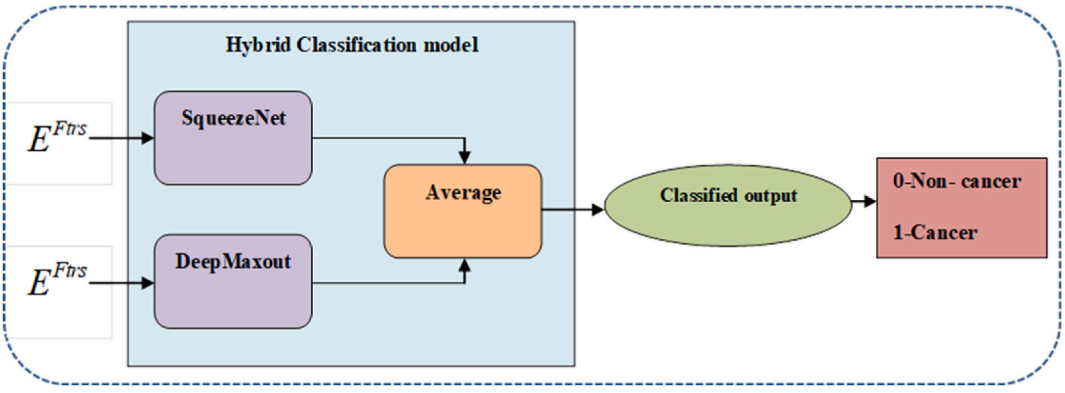

Fig. 5. Pictorial representation of the proposed hybrid classification model.

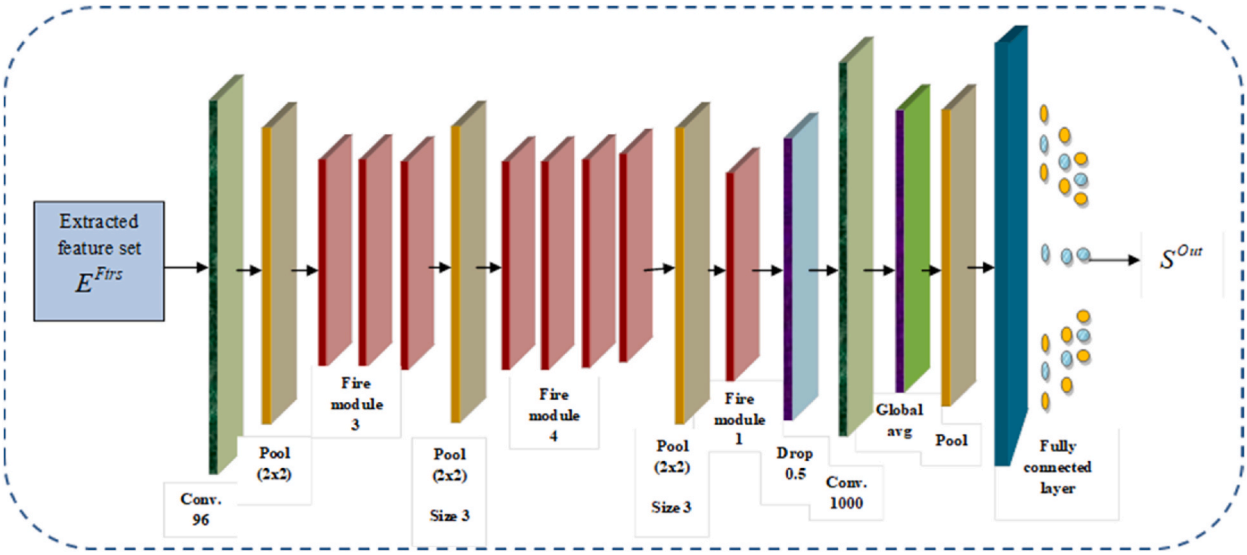

Fig. 6. Architecture of SqueezeNet model.

from the DeepMaxout model can be represented as D^{Out}.

4. Analysis of the liver cancer segmentation and classification model

4.1. Simulation procedure

The proposed liver cancer segmentation and classification were simulated using Python. The Python version used was "Python 3.7," and the processor utilized was "AMD EPYC 7742 64 Core," with an installed RAM capacity of "1.8 TB" Additionally, four NVIDIA A100 (40G) GPUs were used for processing. The liver cancer segmentation and classification analysis were conducted using the two dataset namely Liver Tumor Segmentation dataset and Deep lesion dataset [32,33].

4.2. Dataset description for dataset 1 and dataset 2

Liver cancer is a significant health concern, ranking as the fifth most frequently diagnosed cancer in men and the ninth most common in women. In 2018 alone, there were over 840,000 new cases reported. The liver often becomes a site for both primary and secondary tumor growth, which adds to the complexity of automatically segmenting tumor lesions due to their diverse and diffuse characteristics. Recognizing the importance of this challenge, our work aims to contribute to the advancement of automated segmentation algorithms specifically designed for delineating liver lesions in contrast-enhanced abdominal CT scans. To achieve this goal, we have access to datasets and segmentations provided by multiple clinical facilities around the world. The image dataset is diverse and contains primary and secondary tumors with varied sizes and appearances with various lesion-to-background levels (hyper-/hypo-dense), created in collaboration with seven hospitals and research institutions. The 2D images are utilized in this dataset. Table 2 describes the training and testing images for the dataset. "The DeepLesion dataset contains 32,120 axial computed tomography (CT) slices from 10,594 CT scans (studies) of 4427 unique patients. There are 1–3 lesions in each image with accompanying bounding boxes and size measurements, adding up to 32,735 lesions altogether. The lesion annotations were mined from NIH's picture archiving and communication system (PACS)."

4.3. Performance analysis on dataset 1

The classification evaluation was performed for both the SqueezeNet + DeepMaxout approach and conventional methods. This

Table 2
Training and testing images for liver tumor Segmentation Dataset.

Learning percentage	Testing images	Training images
60 %	(1180, 204)	(1770, 204)
70 %	(885, 204)	(2065, 204)
80 %	(590, 204)	(2360, 204)
90 %	(295, 204)	(2655, 204)

analysis encompassed the assessment of various performance metrics, including specificity, FNR, MCC, accuracy, FPR, F-measure, precision, NPV, and sensitivity. Additionally, we evaluated the effectiveness of adaptive histogram normalization using metrics such as PSNR and SSIM. Furthermore, we compared the performance of the SqueezeNet + DeepMaxout method with state-of-the-art approaches like *m*-RCNN [10], Hybrid ResUNeT [12], SVM [24], and 3D-SDBN [25], as well as traditional methods such as KNN, LSTM, GRU, DeepMaxout, SqueezeNet, and DCNN. Fig. 7(a–f) displays both the original and preprocessed images related to liver cancer. The preprocessed images shown include (a) the original image, (b) Gaussian filtering, (c) median filtering, (d) Wiener filtering, (e) conventional histogram normalization, and (f) adaptive histogram normalization.

Additionally, we conducted a comparative analysis of adaptive histogram normalization with Median Filtering, Gaussian Filtering, Weiner Filtering, and conventional histogram normalization in terms of PSNR and SSIM, as explained in Table 3. It is worth noting that higher PSNR and SSIM values indicate better preprocessing outcomes. The PSNR quantifies the ratio between the highest achievable signal power and the power of disruptive noise affecting the quality of image representation. Among the preprocessing techniques, adaptive histogram normalization achieved the highest PSNR of 33.474, surpassing Median filtering (24.067), Gaussian filtering (23.608), Weiner filtering (19.384), and conventional histogram normalization (30.261). The SSIM assesses the quality of an image by comparing it to a reference image, typically assumed to be flawless. SSIM considers three essential parameters: luminance, contrast, and structural information between the two images. In this regard, the adaptive histogram normalization approach yielded the highest SSIM value of 0.915, outperforming other conventional strategies.

4.4. Segmentation analysis for dataset 1

In the context of liver cancer segmentation evaluation, Fig. 8 provides a series of images related to the segmentation process. These images include the initial input data and the results obtained using various methods (Fig. 8(a–e)), These images include the initial input data and the results obtained using various methods: conventional (b) mr-CNN, (c) FCM, (d) UNet, and (e) the segmented image produced by the proposed cm-RCNN method.

Table 4 presents the segmentation analysis and validation of the proposed cm-RCNN model compared to conventional mr-CNN, FCM, and U-Net models. This analysis involves a comparison between the predicted segmentation and the ground truth. Notably, the proposed cm-RCNN model achieves a high dice score of 0.9295, surpassing the existing models. Furthermore, the Jaccard score, which measures the ratio of the intersection of two sets (predicted and ground truth) to their union, is also discussed. Additionally, the accuracy of the proposed cm-RCNN model is reported at 89.92 %, which is higher than the accuracy of the other models. Qualitative analysis through visual inspection of segmentation results further validates that the proposed cm-RCNN model excels in accurately segmenting the ROI. Experimental results show that compared with other segmentation algorithms, the proposed method improves the Dice value by 0.9716, this high segmentation accuracy offers reduced memory usage and calculation amount. This provides a powerful reference for clinicians to perform liver segmentation.

4.5. Comparative study on positive metrics for dataset 1

Fig. 9(a–c) presents a comparative analysis of positive metrics for liver cancer classification between the SqueezeNet + DeepMaxout method and a set of other models, including KNN, LSTM, GRU, DeepMaxout, SqueezeNet, DCNN, *m*-RCNN [10], Hybrid ResUNeT [12], SVM [24], and 3D-SDBN [25]. Upon a thorough examination of all the positive metric graphs, it becomes evident that the SqueezeNet + DeepMaxout approach outperforms the others, achieving superior values and providing precise classifications for liver cancer. A model's ability to generate higher positive metric values is crucial for accurate liver cancer classification. More precisely, the SqueezeNet + DeepMaxout attains an accuracy of 92.097 at a 70 % training rate. In contrast, traditional approaches yield

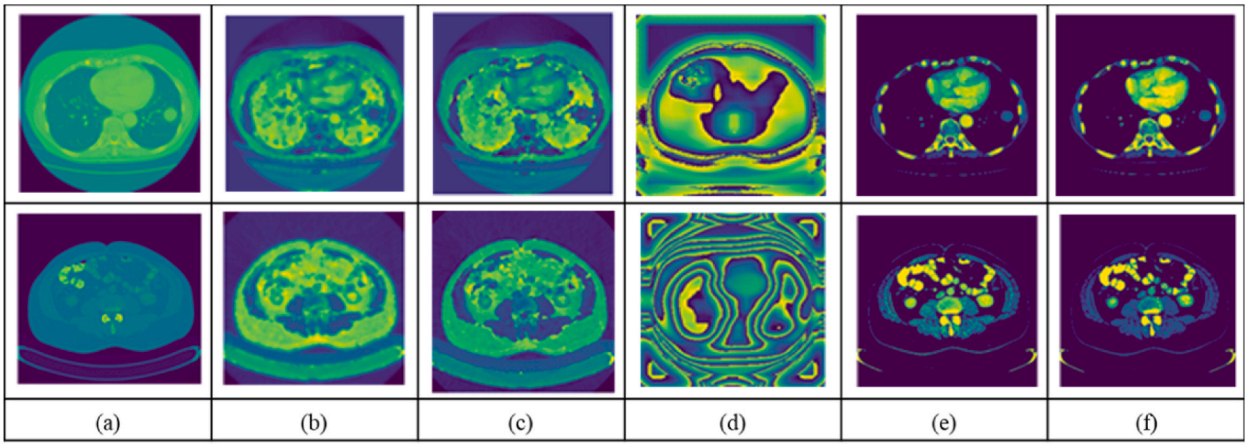

Fig. 7. Preprocessed images for liver cancer: a) original image; b) Gaussian filtering; c) median filtering; d) Wiener filtering; e) conventional histogram normalization; and f) adaptive histogram normalization.

Table 3
PSNR and SSIM analysis on SqueezeNet + DeepMaxout for dataset 1.

Filtering methods	PSNR	SSIM
Median	24.067	0.755
Gaussian	23.608	0.711
Weiner	19.384	0.678
Conventional Histogram Normalization	30.261	0.886
Adaptive Histogram Normalization	33.474	0.915

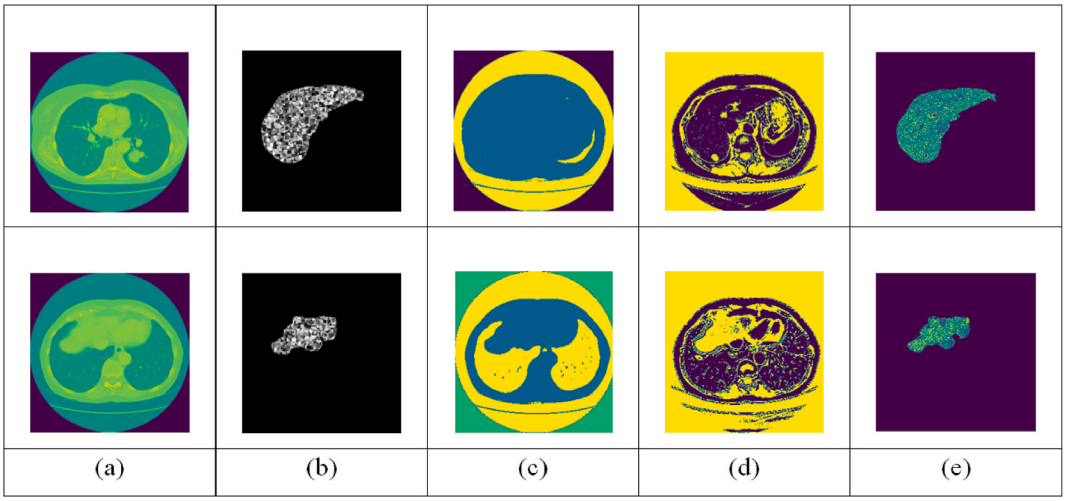

Fig. 8. Segmentation images for liver cancer: a) original image; b) conventional mr-CNN; c) FCM; d) UNet; and e) proposed cm-RCNN segmented image for dataset 1.

Table 4
Dice and Jaccard score analysis on SqueezeNet + DeepMaxout.

Segmentation method	Dice score	Jaccard score	Segmentation accuracy
FCM	0.682338	0.660698	0.690501
UNet	0.641985	0.654867	0.717825
Conventional mr-CNN	0.889037	0.823734	0.885183
proposed cm-RCNN	0.9716	0.9312	0.95002

relatively lower accuracy scores, with KNN at 83.267, LSTM at 84.526, GRU at 82.878, DeepMaxout at 82.195, SqueezeNet at 85.777, DCNN at 67.224, M-RCNN [10] at 81.902, Hybrid ResUNeT [12] at 85.008, SVM at 83.876, and 3D-SDBN at 85.365 respectively. Furthermore, the SqueezeNet + DeepMaxout methodology achieves the highest sensitivity score of 97.698 (training rate = 90), whereas KNN, LSTM, GRU, DeepMaxout, SqueezeNet, DCNN, *m*-RCNN [10], Hybrid ResUNeT [12], SVM, and 3D-SDBN exhibit lower sensitivity ratings.

Simultaneously, the analysis of precision and specificity for both the SqueezeNet + DeepMaxout and conventional strategies is detailed in Fig. 9(b) and (d). Specifically, at a training rate of 60, the SqueezeNet + DeepMaxout achieved a precision score of 93.220, whereas traditional schemes yielded lower precision ratings, with KNN at 83.848, LSTM at 86.114, GRU at 82.694, DeepMaxout at 82.500, SqueezeNet at 84.230, DCNN at 71.562, *m*-RCNN [10] at 84.356, Hybrid ResUNeT [12] at 84.988, SVM at 82.43, and 3D-SDBN at 83.476respectively. In conclusion, the exceptional performance of the SqueezeNet + DeepMaxout methodology ensures its ability to precisely classify liver cancer by utilizing adaptive histogram normalization-based preprocessing, e-MBP-based feature extraction, and a hybrid classification approach. The proposed model delivered excellent results in terms of diagnosing quickly and efficiently. The proposed model is ready for use in detecting liver tumors with accurate liver segmentation.

4.6. Comparative study on negative metrics for dataset 1

To achieve accurate liver cancer classification, negative metrics are evaluated for both the SqueezeNet + DeepMaxout and conventional strategies. This assessment is detailed in Fig. 10. Furthermore, the SqueezeNet + DeepMaxout approach is compared to KNN, LSTM, GRU, DeepMaxout, SqueezeNet, DCNN, *m*-RCNN [10], Hybrid ResUNeT [12], SVM [24], and 3D-SDBN [25]. Minimizing the rate of negative metrics is crucial for efficient liver cancer classification. Notably, at a training rate of 90, the FPR of the SqueezeNet +

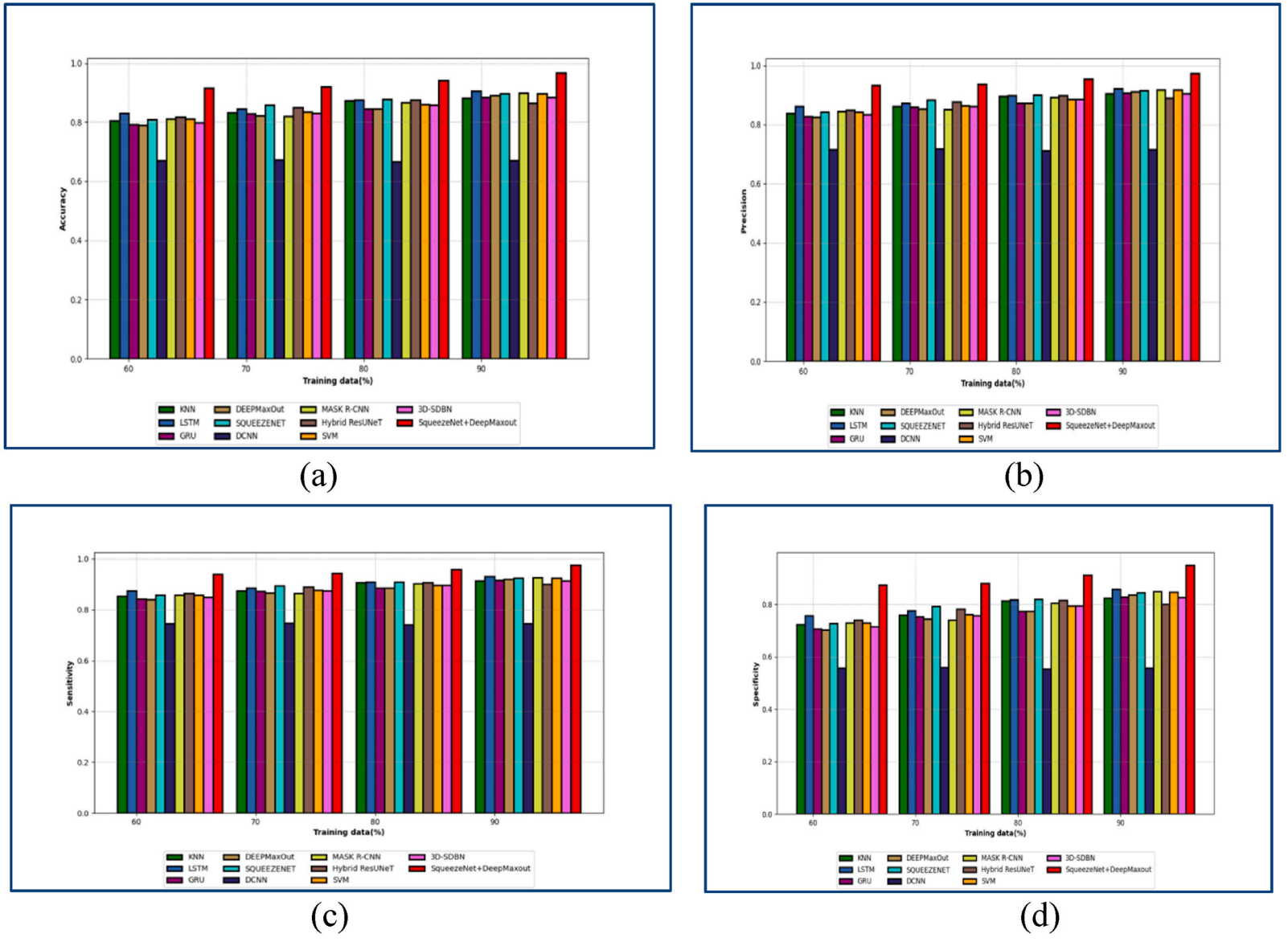

Fig. 9. Assessment of SqueezeNet + DeepMaxout and conventional strategies regarding positive metrics (a) accuracy (b) precision (c) sensitivity (d) specificity.

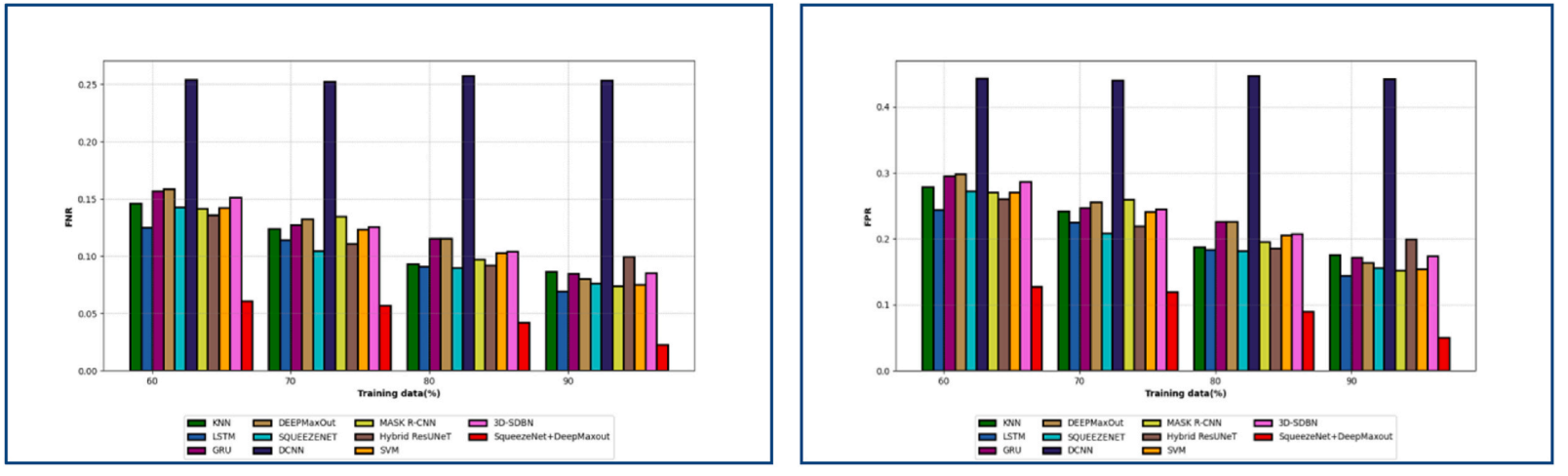

(a) (b)

Fig. 10. Assessment of SqueezeNet + DeepMaxout and conventional strategies regarding negative metrics (a) FNR (b) FPR.

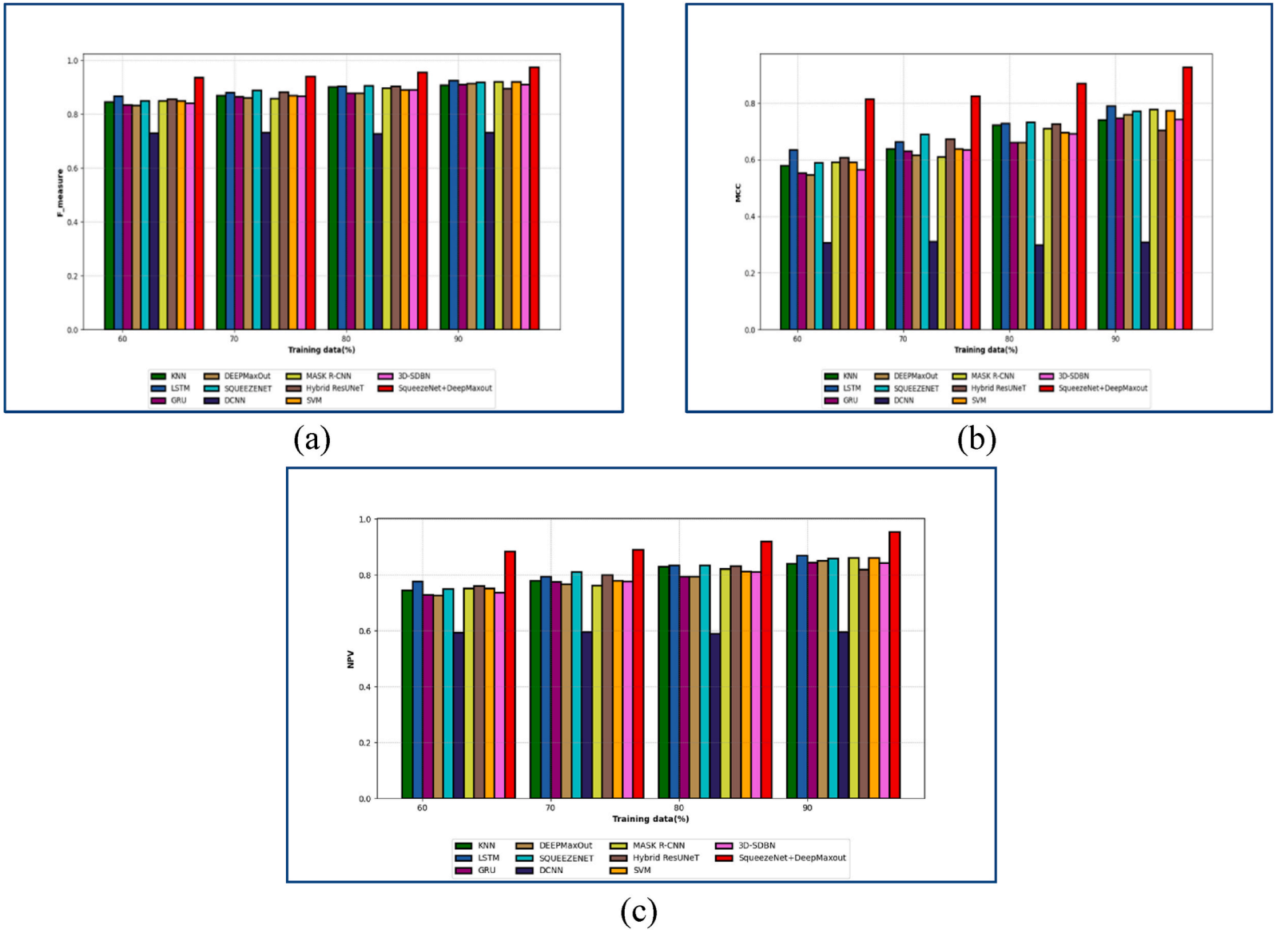

Fig. 11. Assessment of SqueezeNet + DeepMaxout and conventional strategies regarding other metrics (a) F-measure (b) MCC (c) NPV.

DeepMaxout approach is 5.033, significantly lower than KNN (17.579), LSTM (14.403), GRU (17.184), DeepMaxout (16.393), SqueezeNet (15.599), DCNN (44.186), *m*-RCNN [10] (15.201), Hybrid ResUNeT [12] (19.934), SVM (16.543), and 3D-SDBN (15.487) respectively. In Fig. 10(a), the False Negative Rate (FNR) decreases as the training rates improve across all algorithms. However, the SqueezeNet + DeepMaxout method consistently achieves the lowest FNR values across all training rates, as evidenced by the data presented in Fig. 10(b). The SqueezeNet + DeepMaxout approach attains an impressively low False Positive Rate (FPR) of 2.301, whereas KNN, LSTM, GRU, DeepMaxout, SqueezeNet, DCNN, *m*-RCNN [10], Hybrid ResUNeT [12], SVM [24], and 3D-SDBN [25] exhibit comparatively higher FPR values. This indicates that the effectiveness of the SqueezeNet + DeepMaxout approach in classifying liver cancer is indeed higher. This accomplishment can be attributed to the utilization of e-MBP-based feature extraction along with a hybrid classification methodology. The suggested model performed exceptionally well in terms of making diagnoses fast and effectively. With precise liver segmentation, the suggested model is prepared for application in the detection of liver cancers.

4.7. Comparative study on other metrics for dataset 1

To evaluate the effectiveness of liver cancer classification, a comprehensive analysis of various metrics is conducted for the SqueezeNet + DeepMaxout model in comparison to KNN, LSTM, GRU, DeepMaxout, SqueezeNet, DCNN, *m*-RCNN [10], Hybrid ResUNeT [12], SVM [24], and 3D-SDBN [25] as illustrated in Fig. 11(a–c). Comparison of SqueezeNet + DeepMaxout with traditional methods, taking into account supplementary metrics like (Fig. 11(a)) F-measure (Fig. 11(b)), MCC, and (Fig. 11(c)) NPV. Efficient liver cancer classification should yield superior scores in these metrics. When the training rate is 90 %, the SqueezeNet + DeepMaxout approach achieves an impressive MCC of 92.791. In contrast, conventional methods exhibit lower MCC values, including KNN, LSTM, GRU, DeepMaxout, SqueezeNet, DCNN, *m*-RCNN [10], and Hybrid ResUNeT [12]. Specifically, the NPV of the SqueezeNet + DeepMaxout method reaches 91.967 (training rate = 80), while KNN scores 82.969, LSTM scores 83.333, GRU scores 79.343, SqueezeNet scores 83.515, DCNN scores 59.014, *m*-RCNN [10] scores 82.241, Hybrid ResUNeT [12] scores 83.151, SVM scores 82.164, and 3D-SDBN has 84.983 respectively. This demonstrates that the SqueezeNet + DeepMaxout methodology excels in classifying liver cancer. This accomplishment is made possible by the utilization of e-MBP-based feature extraction in combination with a hybrid detection approach. The proposed model performs well in terms of quickly and accurately diagnosing conditions. The proposed model is ready for use in liver cancer detection with accurate liver segmentation.

4.8. Ablation evaluation on SqueezeNet + DeepMaxout

Table 5 provides an ablation assessment of SqueezeNet + DeepMaxout, a conventional preprocessing approach, a model with conventional RCNN, and a conventional MBP for liver cancer classification. Ablation studies are conducted to systematically investigate the impact of integrating or enhancing specific features within the SqueezeNet + DeepMaxout approach. This allows for a more in-depth understanding of the unique contributions made by these features to the overall performance of the SqueezeNet + DeepMaxout framework. In terms of sensitivity, the SqueezeNet + DeepMaxout approach achieves a score of 0.943, while the model with conventional preprocessing scores 0.881, the model with conventional RCNN scores 0.873, and the model with conventional MBP scores 0.892, respectively. Furthermore, the FNR for SqueezeNet + DeepMaxout is 0.057, while the model with conventional preprocessing has an FNR of 0.119, the model with conventional RCNN has an FNR of 0.127, and the model with conventional MBP has an FNR of 0.108. This evaluation demonstrates the enhanced performance of the SqueezeNet + DeepMaxout strategy in liver cancer classification. This improvement can be attributed to the enhanced feature extraction combined with a hybrid classification approach.

4.9. Statistical analysis of accuracy for dataset 1

The statistical evaluation of liver cancer classification models, including SqueezeNet + DeepMaxout, KNN, LSTM, GRU, DeepMaxout, SqueezeNet, DCNN, *m*-RCNN [10], Hybrid ResUNeT [12], SVM [24], and 3D-SDBN [25] is presented in Table 6. Each approach undergoes a comprehensive evaluation to ensure highly accurate estimations. This evaluation includes an analysis of essential statistical metrics, including minimum, median, standard deviation, mean, and maximum values. These metrics collectively offer a comprehensive understanding of the performance and reliability of the studied strategies. For the top statistical metric, the accuracy of the SqueezeNet + DeepMaxout approach is 0.968, whereas KNN achieves 0.882, LSTM attains 0.904, GRU scores 0.884,

Table 5
Comparative ablation study of liver Cancer classification models.

Metrics	Model with conventional preprocessing	Model with conventional RCNN	The model with conventional MBP	SqueezeNet + DeepMaxout
F-measure	0.880	0.871	0.891	0.940
Accuracy	0.871	0.861	0.884	0.921
NPV	0.856	0.845	0.872	0.892
Sensitivity	0.881	0.873	0.892	0.943
FNR	0.119	0.127	0.108	0.057
MCC	0.825	0.809	0.848	0.826
Specificity	0.850	0.838	0.868	0.880
FPR	0.150	0.162	0.132	0.120
Precision	0.878	0.869	0.890	0.936

DeepMaxout reaches 0.890, SqueezeNet obtains 0.896, DCNN scores 0.672, *m*-RCNN [10] achieves 0.899, Hybrid ResUNeT [12] scores 0.874, SVM [24] attains 0.897, and 3D-SDBN [25] obtains 0.883. Similarly, under the median statistical metric, the SqueezeNet + DeepMaxout approach outperforms KNN, LSTM, GRU, DeepMaxout, SqueezeNet, DCNN, *m*-RCNN [10], and Hybrid ResUNeT [12].

4.10. Robustness analysis

Table 7 describes the robustness analysis of the proposed SqueezeNet + DeepMaxout by varying learning rates. The accuracy of the proposed SqueezeNet + DeepMaxout model is 0.920976 which is high when the learning rate is 0.001. Similarly, the proposed model has superior rates in other metrics like sensitivity, specificity, precision, F-measure, MCC, NPV, FPR, and FNR for different learning rates. The suggested model attains a 0.1199 rate for FPR rate which is low in learning rate 0.001. Thus the efficiency of the robustness for the proposed SqueezeNet + DeepMaxout has been demonstrated for the classification of liver tumors using CT images.

4.11. Performance analysis on dataset 2

Both traditional approaches and the SqueezeNet + DeepMaxout methodology were evaluated for classification. Several performance indicators, including as specificity, FNR, MCC, accuracy, FPR, F-measure, precision, NPV, and sensitivity, were evaluated as part of this investigation. Additionally, we used metrics like PSNR and SSIM to assess the efficacy of adaptive histogram normalization. Additionally, we examined how well the SqueezeNet + DeepMaxout method performed in comparison to both conventional techniques like KNN, LSTM, GRU, DeepMaxout, SqueezeNet, and DCNN, and cutting-edge approaches like *m*-RCNN [10], Hybrid ResUNeT [12], SVM [24], and 3D-SDBN [25]. The original and preprocessed images of liver carcinoma are shown in Fig. 12(a-f): Images for liver cancer, with each sub-figure labeled accordingly: (a) original image, (b) after Gaussian filtering, (c) following median filtering, (d) post-conventional histogram normalization, and (e) after Wiener filtering.

Furthermore, as indicated in Table 8, we compared the results of adaptive histogram normalization with conventional histogram normalization and those obtained using median filtering, gaussian filtering, Weiner filtering, and other filters in terms of PSNR and SSIM. It is important to remember that better preprocessing results are indicated by higher PSNR and SSIM values. The PSNR measures the relationship between the maximum signal strength that may be achieved and the disruptive noise power that degrades the quality of the image representation. Adaptive histogram normalization, outperforming conventional histogram normalization (30.413), median filtering (23.405), Gaussian filtering (25.959), Weiner filtering (18.862), and the greatest PSNR of proposed model is (36.529).

4.12. Segmentation analysis on dataset 2

A number of images pertaining to the segmentation procedure are shown in Fig. 13(a-e): (a) the original image, (b) the outcomes of conventional mr-CNN, (c)FCM, (d) UNet, and (e) the proposed cm-RCNN segmented image for dataset 1. These images contain the original input data and the outcomes of several techniques, including the segmented image generated by the suggested cm-RCNN method and the traditional mr-CNN, FCM, and UNet. Table 9 shows the dice and jaccard analysis. The dice coefficient for the proposed model is (~0.96) when compared to the other methods like FCM (~0.72), U-Net (~0.78) and conventional mRCNN (~0.92).

4.13. Comparative study of metrics for dataset 2

An examination of positive metrics, negative metrics and other metrics for classifying liver cancer using the SqueezeNet + DeepMaxout approach and a variety of different models, such as KNN, LSTM, GRU, DeepMaxout, SqueezeNet, DCNN, *m*-RCNN [10], Hybrid ResUNeT [12], SVM [24], and 3D-SDBN [25], is shown in Fig. 14(a–d). When all of the positive metric graphs are carefully examined, it is clear that the SqueezeNet + DeepMaxout method works better than the others, obtaining higher values and offering accurate liver cancer classifications. The capacity of a model to produce greater positive metric values is essential for correctly classifying liver cancer. More specifically, with a 90 % training rate, the SqueezeNet + DeepMaxout achieves an accuracy 97.097. Fig. 14(a–d) presents the assessment of SqueezeNet + DeepMaxout and conventional strategies regarding positive metrics, including

Table 6
Statistical assessment of accuracy.

Method	Standard Deviation	Mean	Median	Max	Min
KNN	0.035868	0.848032	0.852869	0.881604	0.804785
LSTM	0.032576	0.86415	0.86059	0.904202	0.831219
GRU	0.038505	0.837241	0.836544	0.884444	0.791432
DEEPMaxOut	0.042363	0.836392	0.833131	0.89011	0.789197
SQUEEZENET	0.037253	0.860022	0.867557	0.895759	0.809216
DCNN	0.002743	0.669892	0.670677	0.672248	0.665965
MASK R–CNN [10]	0.041475	0.848909	0.843184	0.898578	0.81069
Hybrid ResUNeT [12]	0.024614	0.851775	0.857283	0.874487	0.818047
SVM [24]	0.037316	0.850271	0.84686	0.897156	0.810208
3D-SDBN [25]	0.036574	0.842636	0.844706	0.883024	0.798108
SqueezeNet + DeepMaxout	0.023511	0.936629	0.931356	0.967705	0.916099

Table 7
Robustness analysis of the proposed SqueezeNet + DeepMaxout model.

Learning rate	Accuracy	Sensitivity	Specificity	Precision	F_measure	MCC	NPV	FPR	FNR
0.1	0.91172	0.934669	0.87114	0.927567	0.931093	0.808017	0.882666	0.12886	0.065331
0.01	0.915694	0.93763	0.876863	0.930843	0.934213	0.816613	0.887899	0.123137	0.06237
0.001	0.920976	0.942891	0.880066	0.936208	0.939537	0.825554	0.891952	0.119934	0.057109
0.005	0.912964	0.935536	0.873126	0.928547	0.932016	0.810816	0.884433	0.126874	0.064464

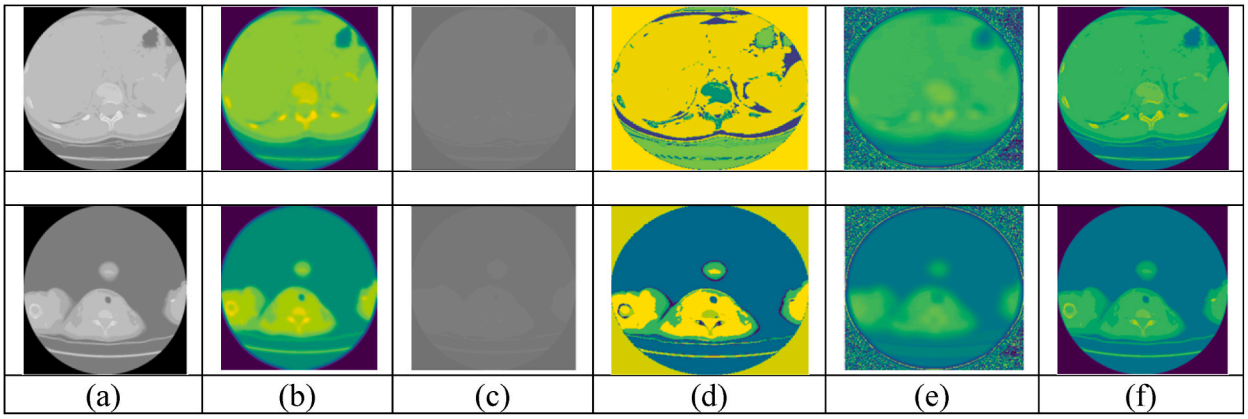

Fig. 12. Images for liver cancer: a) original image; b) Gaussian filtering; c) median filtering; d) conventional histogram normalization e) Wiener filtering(f).

Table 8
PSNR and SSIM analysis on SqueezeNet + DeepMaxout for dataset 1.

Segmentation Method	PSNR	SSIM
Median	23.40518	0.812207
Gaussian	25.95951	0.849875
Weiner	18.86272	0.71783
Conventional histogram equalization	30.41337	0.91953
Proposed histogram equalization	36.52975	0.947743

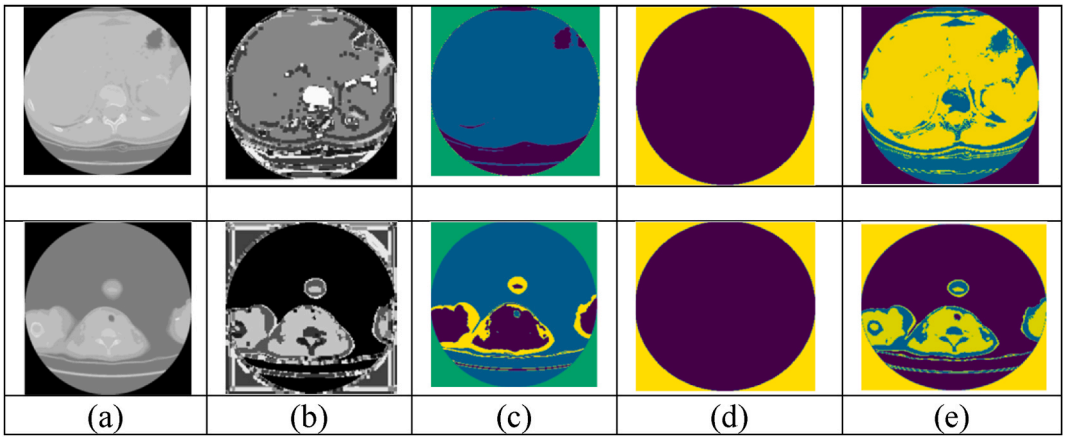

Fig. 13. Segmentation images for liver cancer: a) original image; b) conventional mr-CNN; c) FCM; d) UNet; and e) proposed cm-RCNN segmented image for dataset 1.

(a) accuracy, (b) precision, (c) sensitivity, and (d) specificity. Additionally, Fig. 15(a and b) illustrates the evaluation of SqueezeNet + DeepMaxout and conventional strategies concerning negative metrics, such as (a) False Negative Rate (FNR) and (b) False Positive Rate (FPR). Furthermore, Fig. 16(a–c) depicts the analysis of SqueezeNet + DeepMaxout and conventional strategies regarding other

Table 9
Dice and Jaccard score analysis on SqueezeNet + DeepMaxout.

	FCM	UNet	Conventional_mRCNN	Proposed
dice	0.721868	0.782725	0.922366	0.961648
jaccard	0.700877	0.715221	0.889021	0.92379
segmentation accuracy	0.829786	0.75629	0.918628	0.942273

metrics, including (a) F-measure, (b) Matthews Correlation Coefficient (MCC), and (c) Negative Predictive Value (NPV).

4.14. Analysis of computational time

Table 10 shows the computational time analysis. The computational time of the proposed model is (~63.01) over the existing methods like KNN (~75.52), LSTM (~67.14), GRU (~75.59), Deep maxout (~81.47), Squeezenet (~65.42), DCNN (~66.94), Mask R–CNN (~80.62), Hybrid ResUNet (~79.19), 3D-SDBN (~71.52) and SVM (~63.01). Thus, the superiority of the proposed model is proved over other existing models.

4.15. Analysis on noise vaiance

The trade-off between noise reduction and detail preservation, the selection of filter parameters, the accuracy of edge detection,

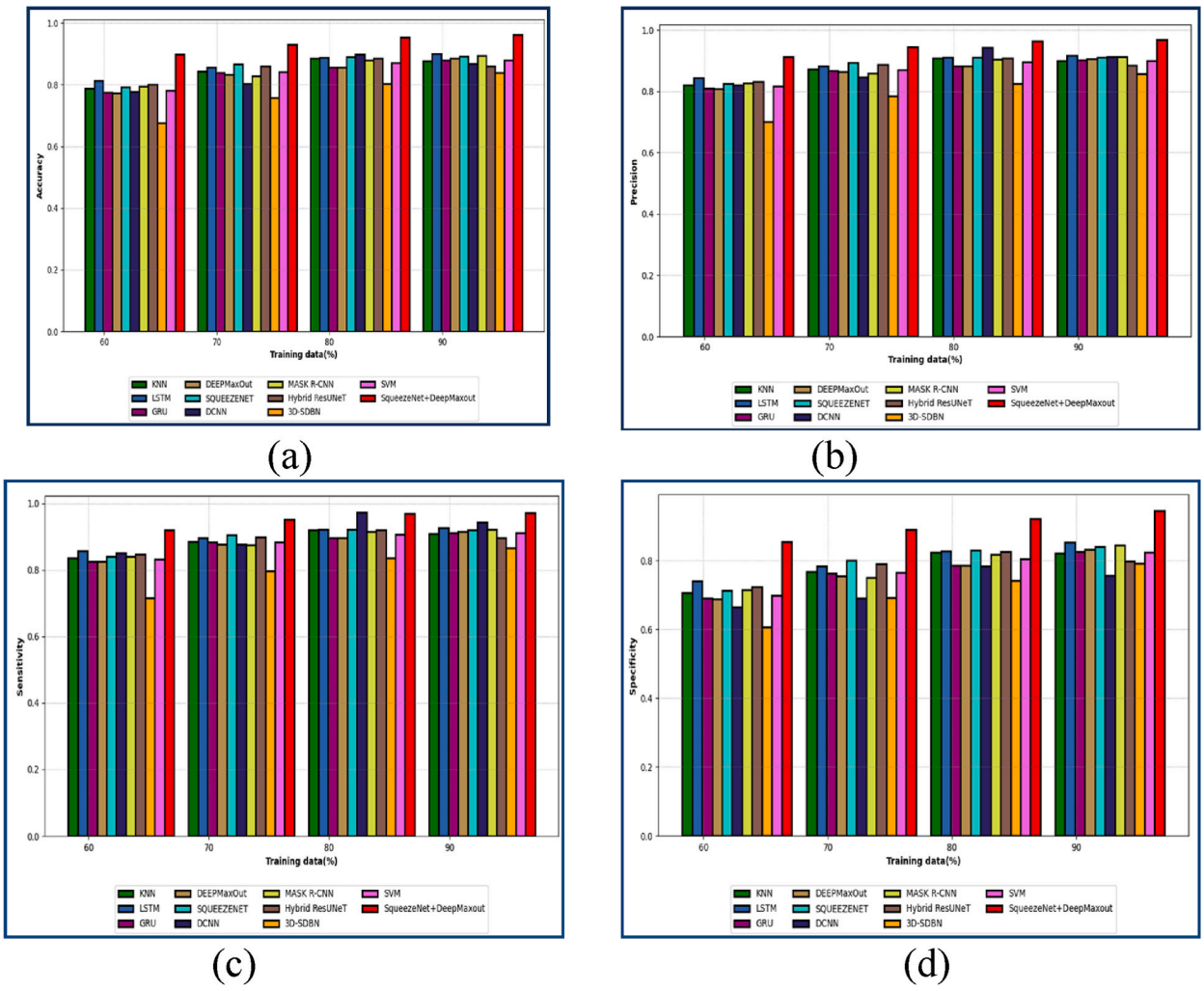

Fig. 14. Assessment of SqueezeNet + DeepMaxout and conventional strategies regarding positive metrics (a) accuracy (b) precision (c) sensitivity (d) specificity.

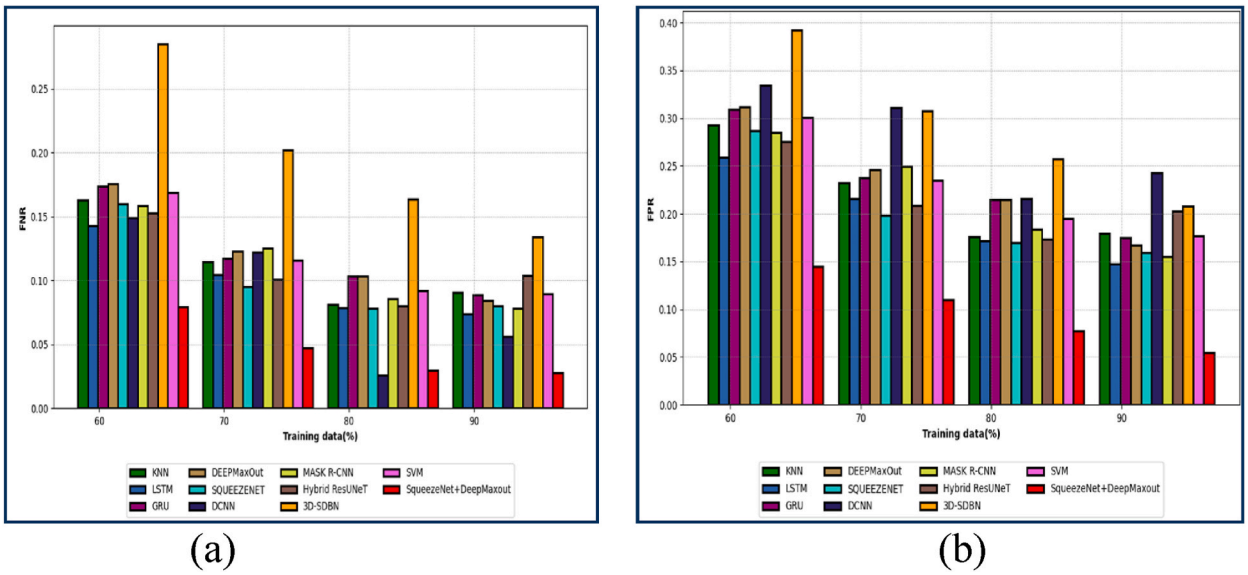

Fig. 15. Assessment of SqueezeNet + DeepMaxout and conventional strategies regarding negative metrics (a) FNR (b) FPR.

and the computational cost of the filtering process are all impacted by noise variance, which has a substantial impact on Gaussian filter performance. Optimizing the filtering process for particular applications can be achieved by modifying the filter parameters, such as the kernel size and standard deviation, based on the noise variance. Table 11 shows the noise variance analysis.

4.16. Analysis on K- fold validation

The method of K-fold cross-validation is used to assess predictive models. There are k folds, or subsets, within the dataset. A distinct fold is used as the validation set for each of the k training and evaluation cycles of the model. The generalization performance of the model is estimated by averaging the performance indicators from each fold. Table 12 shows the K-fold analysis. The f-measure of the proposed model is (~0.94) over the other traditional approaches like KNN, LSTM, GRU, Deepmaxout, Squeezenet, DCNN, Mask R–CNN, Hybrid ResU-NET, 3D-SDBN, and SVM.

4.17. ROC analysis

The ROC curve is used to compare the results of two or more diagnostic tests and to evaluate a test's overall diagnostic performance. It can also be used to choose the best cut-off value to establish if a disease is present or not. Fig. 17 shows the ROC curve analysis. Plotting the true positive rate (TPR) against the false positive rate (FPR) at each threshold setting creates the ROC curve. A helpful method for assessing the efficacy of diagnostic tests and, more broadly, the precision of a statistical model is ROC analysis.

4.18. Limitations

The liver is an intricate organ with a wide range of internal structures, size, and shape. The liver can have tumors in a variety of sites, including difficult spots next to blood arteries or other organs. Such intricate anatomical circumstances may make it difficult for segmentation algorithms to distinguish malignancies with accuracy.Different kinds of noise, abnormalities, and distortions can be seen in medical images of the liver due to patient mobility, flaws in the scanner, and differences in the imaging technique. Tumor delineation may become erroneous due to segmentation algorithms' inability to withstand noise and artifacts. It frequently takes an interdisciplinary team effort including computer scientists, medical imaging specialists, physicians, and regulatory experts to address these problems. Additionally, it calls for the creation of reliable, clinically verified segmentation algorithms that are adapted to the unique needs and limitations.

4.19. Practical implications

In medical imaging applications including radiation planning, post-treatment evaluation, and surgical planning, segmenting the liver and liver lesions is a crucial step. Our proposed system can verify the results on CT-scan databases, which could help radiologists to diagnose liver tumors. It is a reliable and effective method that may be used on huge clinical datasets to lower human error. The suggested approach preserved accuracy while being effective. Without appreciably increasing the processing time, such a quick segmentation technique might be used for real-world uses like radiofrequency ablation trajectory planning, which entails segmenting

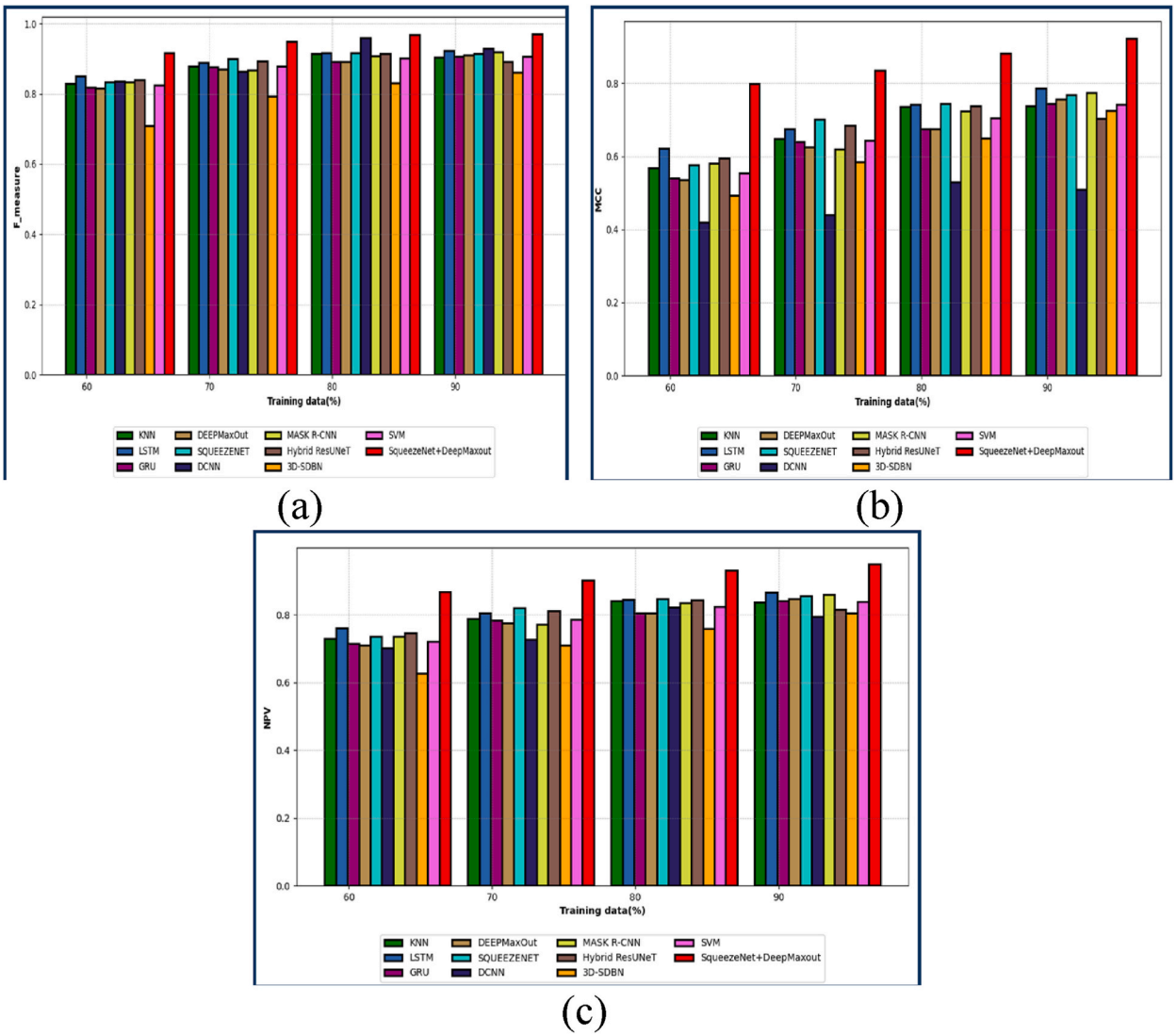

Fig. 16. Assessment of SqueezeNet + DeepMaxout and conventional strategies regarding other metrics (a) F-measure (b) MCC (c) NPV.

Table 10
Computational time analysis.

Methods	Computing Time(s)
KNN	75.5207
LSTM	67.14659
GRU	75.59414
DEEPMaxOut	81.4787
SQUEEZENET	65.42338
DCNN	66.9475
MASK R–CNN	80.62917
Hybrid ResUNeT	79.19388
3D-SDBN	71.5254
SVM	69.32599
SqueezeNet + DeepMaxout	63.01553

all pertinent organs and structures. Furthermore, several real-time treatment planning applications, including thermal percutaneous ablation, percutaneous ethanol injection (PEI), radiotherapy surgical resection, and arterial embolism, are made possible by the segmentation and categorization of liver tumors.

Table 11
Noise variance analysis.

	Accuracy	Sensitivity	Specificity	Precision	F_measure	MCC	NPV	FPR	FNR
gaussian-noise = 0.1	0.941	0.953937	0.91776	0.950192	0.952061	0.88833	0.924774	0.08224	0.046063
gaussian-noise = 0.2	0.937742	0.950064	0.914033	0.946333	0.948195	0.884723	0.921019	0.085967	0.049936
gaussian-noise = 0.3	0.937551	0.94987	0.913847	0.94614	0.948001	0.884542	0.920831	0.086153	0.05013

Table 12
K-fold validation analysis.

	Accuracy	Sensitivity	Specificity	Precision	F_measure	MCC	NPV	FPR
KNN	0.8389	0.8803	0.7671	0.8674	0.8736	0.651	0.787	0.2328
LSTM	0.8535	0.8918	0.7862	0.8800	0.8858	0.681	0.805	0.2137
GRU	0.8178	0.8639	0.7392	0.8496	0.8567	0.606	0.761	0.2607
DEEPMaxOut	0.8167	0.8630	0.7377	0.8486	0.8558	0.604	0.759	0.2622
SQUEEZENET	0.8432	0.8837	0.7729	0.8711	0.8774	0.660	0.792	0.2270
DCNN	0.8390	0.8805	0.76701	0.8676	0.8740	0.651	0.787	0.2329
MASK R–CNN	0.8773	0.9101	0.8183	0.9000	0.9050	0.731	0.835	0.1817
Hybrid ResUNeT	0.8559	0.8936	0.7897	0.8819	0.8877	0.686	0.808	0.2102
3D-SDBN	0.8462	0.8861	0.7766	0.8737	0.8799	0.666	0.796	0.2233
SVM	0.6681	0.7440	0.5547	0.7136	0.7285	0.302	0.592	0.4452
SqueezeNet + DeepMaxout	0.9289	0.9487	0.89177	0.9426	0.94569	0.842	0.902	0.1082

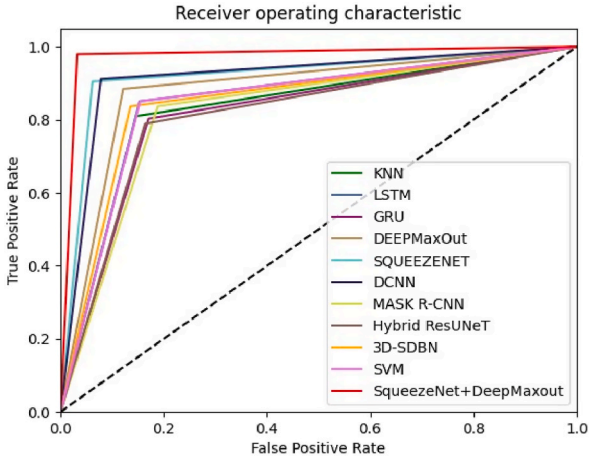

Fig. 17. Analysis on ROC curve.

5. Conclusion

This paper presents a novel framework for liver cancer segmentation and classification, comprising the following key steps: preprocessing, segmentation, feature extraction, and classification. The initial liver image undergoes preprocessing, where AHE is applied. Within AHE, several enhancements are performed, including dehazing, color distortion removal, and linear transformation, resulting in the preprocessed image. Subsequently, the precise ROI corresponding to the liver is segmented from this preprocessed image, achieved through an innovative deep strategy named cm-RCNN. Activation functions such as ReLU and *m*-Sig are employed during this process. From the segmented image, a variety of features are extracted, including ResNet features, shape features (such as area, perimeter, approximation, and convex hull), and e-MBP-based features. These extracted features are then utilized in a hybrid classification model that incorporates classifiers like SqueezeNet and DeepMaxout models. The classification outcome is determined by taking the average of the scores obtained from both classifiers. The proposed SqueezeNet + DeepMaxout attains an accuracy of 92.097 at a 70 % training rate while traditional approaches yield relatively lower accuracy scores, with KNN at 83.267, LSTM at 84.526, GRU at 82.878, DeepMaxout at 82.195, SqueezeNet at 85.777, DCNN at 67.224, M-RCNN at 81.902, Hybrid ResUNeTat 85.008, SVM at 83.876, and 3D-SDBN at 85.365, respectively. Consequently, the SqueezeNet + DeepMaxout approach has 0.968, whereas KNN achieves 0.882, LSTM attains 0.904, GRU scores 0.884, DeepMaxout reaches 0.890, SqueezeNet obtains 0.896, DCNN scores 0.672, *m*-RCNN achieves 0.899, Hybrid ResUNeTscores 0.874, SVM attains 0.897, and 3D-SDBN obtains 0.883 in maximum statistical measures. The suggested model performed exceptionally well in terms of making diagnoses fast and effectively. Additionally, the rate of DC authentication increased, indicating that the experiment proceeded successfully and the model is prepared for use in liver tumor

detection. But when it comes to lesions or tumors at the liver boundary, the suggested strategy is prone to small over- or under-segmentation errors. Although the suggested methodology produced some encouraging results, it can still be improved. Since the proposed method is based on a 2D network and the CT scans are 3D, it can easily lose important context information along the z-axis. Additionally, in cases where the liver margin has tumor abnormalities or lesions, the suggested approach may result in significant errors around the boundary. In order to minimize inaccuracies, our future work will focus on fully exploiting the 3D z-axis information. In the future, this work will extended by applying the same model with more optimized parametric selection on other organs such as kidney segmentation, and brain tumor segmentation problems.

Data availability

The data presented in the figures within this paper and other findings of this study are available from the corresponding author, (Bingding Huang, huangbingding@sztu.edu.cn), upon reasonable request. Additionally, the public datasets use in this study are referenced as follows:

LiTS [32]: Liver Tumor Segmentation dataset. https://www.kaggle.com/datasets/andrewmvd/liver-tumor-segmentation?select=volume_pt1. DeepLesion dataset [33]. https://nihcc.box.com/v/DeepLesion.

Code availability

The custom codes used to produce the results presented in this paper are available from the corresponding authors upon reasonable request.

CRediT authorship contribution statement

Rashid Khan: Writing – review & editing, Writing – original draft, Validation, Software, Methodology, Investigation, Funding acquisition, Formal analysis, Data curation, Conceptualization. **Liyilei Su:** Writing – review & editing, Visualization, Software. **Asim Zaman:** Writing – review & editing, Software, Formal analysis. **Haseeb Hassan:** Writing – review & editing, Investigation, Data curation. **Yan Kang:** Writing – review & editing, Supervision, Conceptualization. **Bingding Huang:** Writing – review & editing, Supervision, Software, Methodology, Funding acquisition, Conceptualization.

Declaration of competing interest

The authors declare that they have no known competing financial interests or personal relationships that could have appeared to influence the work reported in this paper.

Acknowledgments

This study was supported by the Project of the Educational Commission of Guangdong Province of China (No. 2022ZDJS113).

References

[1] R.L. Siegel, K.D. Miller, N.S. Wagle, A. Jemal, Cancer statistics, 2023, Ca-Cancer J. Clin. 73 (2023) 17–48.
[2] M.Y. Ansari, A. Abdalla, M.Y. Ansari, M.I. Ansari, B. Malluhi, S. Mohanty, S. Mishra, S.S. Singh, J. Abinahed, A. Al-Ansari, Practical utility of liver segmentation methods in clinical surgeries and interventions, BMC Med. Imag. 22 (2022) 1–17.
[3] M. Ahmad, D. Ai, G. Xie, S.F. Qadri, H. Song, Y. Huang, Y. Wang, J. Yang, Deep belief network modeling for automatic liver segmentation, IEEE Access 7 (2019) 20585–20595.
[4] D. Rajput, B. Bejoy, Optimized deep maxout for breast cancer detection: consideration of pre-treatment and in-treatment aspect, Multimed. Tool. Appl. (2023) 1–31. DOI.
[5] C. Sun, A. Xu, D. Liu, Z. Xiong, F. Zhao, W. Ding, Deep learning-based classification of liver cancer histopathology images using only global labels, IEEE J Biomed Health Inform 24 (2019) 1643–1651.
[6] B. Lakshmipriya, B. Pottakkat, G. Ramkumar, Deep learning techniques in liver tumour diagnosis using CT and MR imaging-A systematic review, Artif. Intell. Med. (2023) 102557. DOI.
[7] V. Nainamalai, P.J.R. Prasad, E. Pelanis, B. Edwin, F. Albregtsen, O.J. Elle, R.P. Kumar, Evaluation of clinical applicability of automated liver parenchyma segmentation of multi-center magnetic resonance images, Eur J Radiol Open 9 (2022) 100448.
[8] H. Zhang, L. Guo, D. Wang, J. Wang, L. Bao, S. Ying, H. Xu, J. Shi, Multi-source transfer learning via multi-kernel support vector machine plus for B-mode ultrasound-based computer-aided diagnosis of liver cancers, IEEE Trans. Ultrason. Ferroelectrics Freq. Control 25 (2021) 3874–3885.
[9] N.N. Prakash, V. Rajesh, D.L. Namakhwa, S.D. Pande, S.H. Ahammad, A DenseNet CNN-based liver lesion prediction and classification for future medical diagnosis, Sci African 20 (2023) e01629.
[10] P.K. Balasubramanian, W.-C. Lai, G.H. Seng, J. Selvaraj, Apestnet with mask r-cnn for liver tumor segmentation and classification, Cancers 15 (2023) 330.
[11] N.G. Rognin, M. Arditi, L. Mercier, P.J. Frinking, M. Schneider, G. Perrenoud, A. Anaye, J.-Y. Meuwly, F. Tranquart, Parametric imaging for characterizing focal liver lesions in contrast-enhanced ultrasound, IEEE Trans. Ultrason. Ferroelectrics Freq. Control 57 (2010) 2503–2511.
[12] H. Rahman, T.F.N. Bukht, A. Imran, J. Tariq, S. Tu, A. Alzahrani, A deep learning approach for liver and tumor segmentation in CT images using ResUNet, Bioengineering 9 (2022) 368.
[13] S. Kierner, J. Kucharski, Z. Kierner, Taxonomy of hybrid architectures involving rule-based reasoning and machine learning in clinical decision systems: a scoping review, J. Biomed. Inf. (2023) 104428. DOI.
[14] J. Munoz-Gama, N. Martin, C. Fernandez-Llatas, O.A. Johnson, M. Sepúlveda, E. Helm, V. Galvez-Yanjari, E. Rojas, A. Martinez-Millana, D. Aloini, Process mining for healthcare: characteristics and challenges, J. Biomed. Inf. 127 (2022) 103994.
[15] J. Ma, Y. Deng, Z. Ma, K. Mao, Y. Chen, A liver segmentation method based on the fusion of VNet and WGAN, Comput. Math. Methods Med. 2021 (2021) 1–12.

[16] W. Tang, D. Zou, S. Yang, J. Shi, J. Dan, G. Song, A two-stage approach for automatic liver segmentation with Faster R-CNN and DeepLab, Neural Comput. Appl. 32 (2020) 6769–6778.
[17] K. Wang, A. Mamidipalli, T. Retson, N. Bahrami, K. Hasenstab, K. Blansit, E. Bass, T. Delgado, G. Cunha, M.S. Middleton, Automated CT and MRI liver segmentation and biometry using a generalized convolutional neural network, Radiol Artif Intell 1 (2019) 180022.
[18] H. Zhang, X. Yang, D. Li, Y. Cui, J. Zhao, S. Qiu, Dual parallel net: a novel deep learning model for rectal tumor segmentation via CNN and transformer with Gaussian Mixture prior, J. Biomed. Inf. 139 (2023) 104304.
[19] F. Shamshad, S. Khan, S.W. Zamir, M.H. Khan, M. Hayat, F.S. Khan, H. Fu, Transformers in medical imaging: a survey, Med. Image Anal. (2023) 102802. DOI.
[20] A.E. Kavur, N.S. Gezer, M. Barış, Y. Şahin, S. Özkan, B. Baydar, U. Yüksel, Ç. Kılıkçıer, Ş. Olut, G.B. Akar, Comparison of semi-automatic and deep learning-based automatic methods for liver segmentation in living liver transplant donors, Diagn Interv Radiol 26 (2020) 11.
[21] D.C. Le, K. Chinnasarn, J. Chansangrat, N. Keeratibharat, P. Horkaew, Semi-automatic liver segmentation based on probabilistic models and anatomical constraints, Sci. Rep. 11 (2021) 6106.
[22] Y. Zhou, Q. Kong, Y. Zhu, Z. Su, MCFA-UNet: multiscale cascaded feature attention U-Net for liver segmentation, IRBM (2023) 100789. DOI.
[23] E. Trivizakis, G.C. Manikis, K. Nikiforaki, K. Drevelegas, M. Constantinides, A. Drevelegas, K. Marias, Extending 2-D convolutional neural networks to 3-D for advancing deep learning cancer classification with application to MRI liver tumor differentiation, IEEE J Biomed Health Inform 23 (2018) 923–930.
[24] N.N. Reddy, G. Ramkumar, Liver segmentation and classification in computed tomography images using convolutional neural network and comparison of accuracy with support vector machine, in: AIP Conf Proc, AIP Publishing, 2023.
[25] J. Dickson, A. Linsely, R.A. Nineta, An integrated 3D-sparse deep belief network with enriched seagull optimization algorithm for liver segmentation. Multimed Syst, 2023, pp. 1–20.
[26] R. Manjunath, K. Kwadiki, Automatic liver and tumour segmentation from CT images using Deep learning algorithm, Results Control Optim 6 (2022) 100087.
[27] S.H. Forrest N. Iandola, Matthew W. Moskewicz, Khalid Ashraf, William J. Dally, Kurt Keutzer, SqueezeNet: AlexNet-level accuracy with 50x fewer parameters and <0.5MB model size, ICLR (2017).
[28] A.M. Benjamin Bancher, Isabella ellinger, improving mask R-CNN for nuclei instance segmentation in hematoxylin & eosin-stained histological images, in: MICCAI Workshop Comput. Pathol., 2021.
[29] A. Hafiane, K. Palaniappan, G. Seetharaman, Joint adaptive median binary patterns for texture classification, Pattern Recogn. 48 (8) (2015) 2609–2620.
[30] O.A. Fadipe-Joseph, A.T. Oladipo, U.A. Ezeafulukwe, Modified sigmoid function in univalent function theory, Int. J. Math. Sci. Eng. Appl 7 (2013) 313–317.
[31] J. Liu, Y. Shi, Image feature extraction method based on shape characteristics and its application, in: Medical Image Analysis, Springer Berlin Heidelberg, Berlin, Heidelberg, 2011, pp. 172–178.
[32] P. Bilic, P. Christ, H.B. Li, E. Vorontsov, A. Ben-Cohen, G. Kaissis, A. Szeskin, C. Jacobs, G.E.H. Mamani, G. Chartrand, The liver tumor segmentation benchmark (lits), Med. Image Anal. 84 (2023) 102680.
[33] K. Yan, X. Wang, L. Lu, R.M. Summers, DeepLesion: automated mining of large-scale lesion annotations and universal lesion detection with deep learning, J. Med. Imaging 5 (2018), 036501-036501.